© 2018. Published by The Company of Biologists Ltd | Journal of Cell Science (2018) 131, jcs205807. doi:10.1242/jcs.205807

RESEARCH ARTICLE

Aplip1, the *Drosophila* homolog of JIP1, regulates myonuclear positioning and muscle stability

Alexander L. Auld, Sacha A. Roberts, Ciaran B. Murphy, Jaclyn M. Camuglia and Eric S. Folker*

ABSTRACT

During muscle development, myonuclei undergo a complex set of movements that result in evenly spaced nuclei throughout the muscle cell. In *Drosophila*, two separate pools of Kinesin and Dynein work in synchrony to drive this process. However, how these two pools are specified is not known. Here, we investigate the role of Aplip1 (the *Drosophila* homolog of JIP1, JIP1 is also known as MAPK8IP1), a known regulator of both Kinesin and Dynein, in myonuclear positioning. Aplip1 localizes to the myotendinous junction and has genetically separable roles in myonuclear positioning and muscle stability. In *Aplip1* mutant embryos, there was an increase in the percentage of embryos that had both missing and collapsed muscles. Via a separate mechanism, we demonstrate that Aplip1 regulates both the final position of and the dynamic movements of myonuclei. Aplip1 genetically interacts with both Raps (also known as Pins) and Kinesin to position myonuclei. Furthermore, Dynein and Kinesin localization are disrupted in Aplip1 mutants suggesting that Aplip1-dependent nuclear positioning requires Dynein and Kinesin. Taken together, these data are consistent with Aplip1 having a function in the regulation of Dynein- and Kinesin-mediated pulling of nuclei from the muscle end.

This article has an associated First Person interview with the first author of the paper.

KEY WORDS: Aplip1, Jip1, Nuclear movement, Muscle, Kinesin, Dynein

INTRODUCTION

Actively positioning organelles has been demonstrated to be an important process in the development of naturally polarized cells such as epithelial cells, cell migration and neuronal outgrowth among other cellular functions (van Bergeijk et al., 2016). One of the more dramatic examples of cellular organization is the precise positioning of the many nuclei within the skeletal muscle syncytium. Beyond the striking appearance of evenly distributed nuclei throughout the periphery of a large cell, the mechanism of myonuclear positioning has gained interest in recent years because mispositioned nuclei in muscle correlate with a variety of muscle diseases (Iyer et al., 2017; Jeannet et al., 2004; Meinke et al., 2014). Although this correlation has been noted for decades (Spiro et al., 1966), the mechanisms and functions of myonuclear movement in muscle have only recently begun to emerge.

During muscle development, myonuclei undergo a complex set of movements to maximize the internuclear distance at the periphery of the muscle cell (Bruusgaard et al., 2006; Cadot et al., 2012; Wilson and Holzbaur, 2012, 2015). Although experiments with mammalian cell culture systems have shed light on some of the mechanisms that govern myonuclear positioning, they do not recapitulate the constraints of development in an organism. *In vivo* analysis of myonuclear movement during muscle development in mammals is difficult because functional muscles are a complex set of bundled bundles of muscle cells. To overcome this limitation, we use embryonic muscle development in *Drosophila melanogaster* as a model system. In addition to being a powerful genetic system, *Drosophila* is a powerful cell biological system in which each individual muscle cell is a fully functional muscle. This simplicity makes *Drosophila* muscle development optically tractable. Despite the differences in the organization of the muscle cells relative to one another, the structure of the individual muscle cells is highly conserved between *Drosophila* and mammals (Bruusgaard et al., 2006; Metzger et al., 2012; Rai et al., 2014; Weitkunat et al., 2014).

Nuclear movement in *Drosophila* is a multi-step process that can be divided into at least three distinct phases. After fusion, nuclei are clustered off-center toward the ventral end of the muscle [10:20–11:20 h after egg laying (AEL)]. The first movement is the splitting of this large cluster of nuclei into two separate groups of nuclei. Second, the two separate groups move directionally, with one moving toward the ventral end of the muscle and the other toward the dorsal end of the muscle (11:20–16 h AEL). Third, after the distance between the two groups of nuclei has reached its maximum, the nuclei move back into the center and evenly distribute throughout the muscle (16–20 h AEL) (Folker et al., 2012; Metzger et al., 2012).

Previous work in *Drosophila* has demonstrated that myonuclear movement is dependent on two spatially segregated Kinesin and Dynein pathways (Folker et al., 2012, 2014; Schulman et al., 2014). One pathway, termed the proximal pathway, involves Kinesin and Dynein exerting force directly on the nucleus. Kinesin pulls the front of the nucleus to create a leading edge while Dynein acts on the lagging edge of the nucleus. This polarization of Kinesin and Dynein activity drives dynamic changes in the shape of the nucleus as it moves toward the muscle end (Folker et al., 2014). The second pathway, termed the cortical pathway, involves the cytoskeleton-dependent generation of force from the muscle end. Briefly, plus-ends of microtubules that are nucleated at the myonuclear envelope interact with the cell cortex in a CLIP-190-dependent manner. Kinesin transports Dynein to the cell cortex along these microtubules where Dynein is anchored by Raps (also known as Pins). This allows Dynein to pull the minus-ends of microtubules toward the muscle pole. These two mechanisms appear to occur simultaneously. Therefore, how each pool of motors is specified and how each motor is regulated within a pathway are crucial questions to understanding the mechanisms of myonuclear movement.

Kinesin and Dynein are regulated by several mechanisms in distinct signaling pathways, including JNK signaling. Specifically, Kinesin and Dynein are coordinated by JNK-interacting proteins (JIPs).

Department of Biology, Boston College, Chestnut Hill, MA 02467, USA.

*Author for correspondence (eric.folker@bc.edu)

E.S.F., 0000-0003-1619-7330

Received 3 May 2017; Accepted 7 February 2018

Journal of Cell Science (2018) 131, jcs205807. doi:10.1242/jcs.205807

JIP-dependent motor regulation is critical for transport of cargoes in axons (Cavalli et al., 2005; Fu and Holzbaur, 2013; Horiuchi et al., 2005). Additionally, JIP3 (also known as Syd in flies and MAPK8IP3 in mammals) contributes to myonuclear postion in *Drosophila* via regulation of Kinesin-dependent transport of Dynein (Schulman et al., 2014). In muscle, Syd facilitates Kinesin-dependent transport of Dynein to the muscle end (Schulman et al., 2014). However, these data left many questions, including how Kinesin and Dynein are coordinated to apply force directly to the nucleus, and how Dynein activity is regulated when it is at the muscle end.

Another cytoskeleton-dependent behavior that is regulated at the end of the muscle is the development of the myotendinous junction (MTJ). This specialized cell–cell attachment is essential for the stability of the muscle and the transmission of force from the muscle cell to the skeleton. As the cell grows, it extends filopodia-like projections from the muscle pole to connect with the correct tendon cell (Weitkunat et al., 2014). Once bound, transmembrane proteins, such as β-integrins, cluster at the muscle end and make a stable attachment (Bao et al., 1993; Pines et al., 2012; Volk et al., 1990). Cytoskeleton-dependent MTJ development occurs at the same time and place that the cytoskeleton-dependent force is being generated to move nuclei. Thus, whether some molecules might be used in, and coordinate both processes, is an intriguing question.

We therefore investigated the function of *Aplip1* (the *Drosophila* JIP1; JIP1 is also known as MAPK8IP1 in mammals) during muscle development. Aplip1 is one of two JIP proteins in *Drosophila* (Syd is the other) (Taru et al., 2002). Aplip1/JIP1 only has one motor-binding domain, which is regulated to shuffle JIP1 between Kinesin and Dynein binding states. This makes Aplip1 a candidate for organizing the microtubule motors to move a large organelle like the nucleus, as the coordination of both motors is important in progressively moving the nucleus in one direction (Fu and Holzbaur, 2013; Horiuchi et al., 2005, 2007).

Here, we demonstrate that Aplip1 regulates both myonuclear positioning and muscle attachment. With respect to myonuclear positioning, *Aplip1* genetically interacts with *Khc* and *Raps* suggesting that it operates within the already described pathways for the regulation of myonuclear movement. However, Aplip1 does not interact with any of the known regulators of myonuclear movement to regulate muscle attachment. Thus, *Aplip1* may represent a critical node that coordinates the positioning of nuclei and the structure of the myotendinous junction.

RESULTS

Aplip1 localizes to myotendinous junctions

To determine where Aplip1 is localized during early muscle development in the *Drosophila* embryo, we expressed Aplip1–eGFP via the UAS system specifically in the mesoderm by using *Twsit-Gal4* (Greig and Akam, 1993). Aplip1–eGFP localized to the cell ends near the MTJs. Embryos were stained for both Aplip–eGFP and β-PS-integrin (also known as Myospheroid). The signals were closely associated and confirmed that there was an accumulation of Aplip1 near the MTJ (Fig. 1A–C). Live embryo time-lapse microscopy of Aplip1–eGFP indicated that Aplip1 localized in

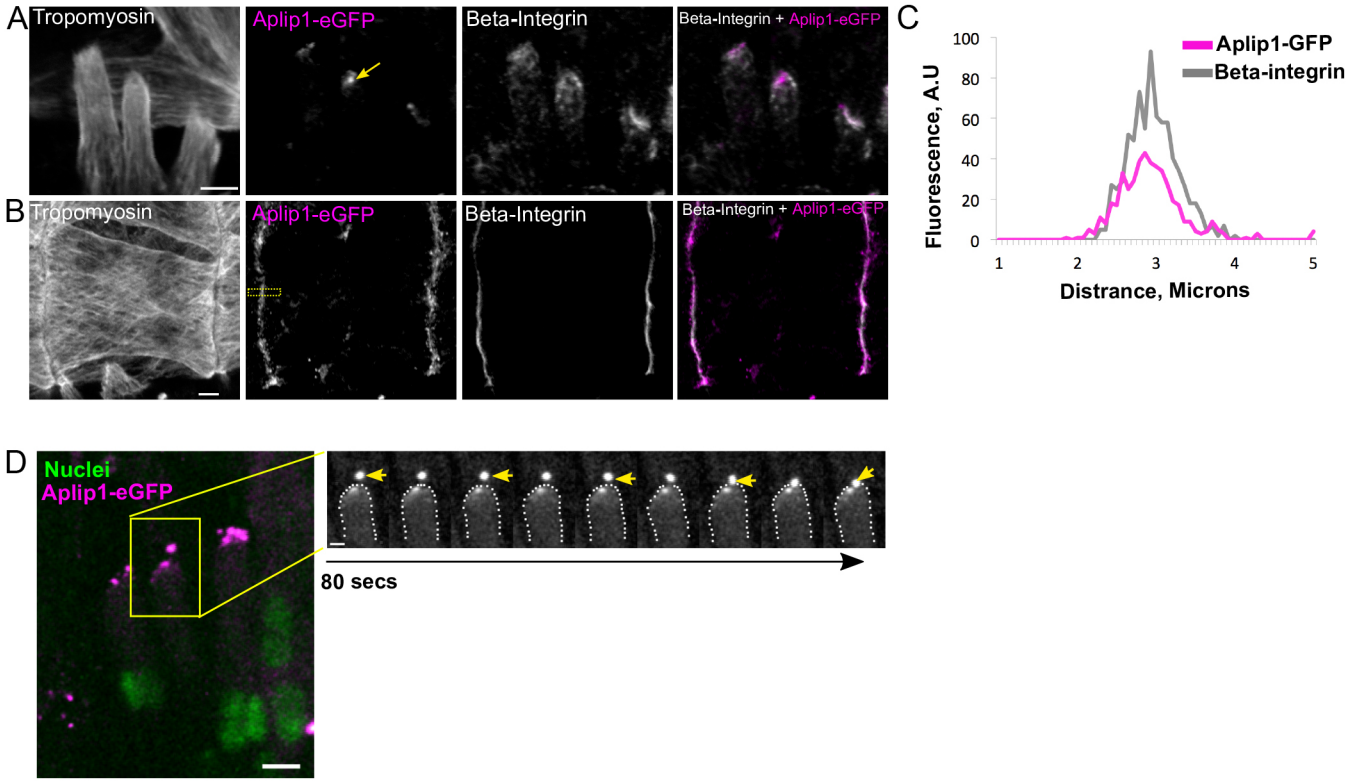

Fig. 1. Aplip1 colocalizes with β-integrin in *Drosophila* muscle. (A,B) Immunofluorescence images of the dorsal tips of the LT muscles (A) or the entire Dorsal muscle 2 (B) in stage 16 embryos. Muscles are shown via indirect immunofluorescence tropomyosin staining (gray). Aplip1–eGFP, magenta; β-integrin (gray). The yellow arrow (A) indicates Aplip1–eGFP localizing to the LT muscle pole. Scale bars: 5 µm. (C) Intensity profile taken through the middle of yellow box in B for both Aplip1–eGFP (magenta) and β-integrin (gray) showing localization of Aplip1–eGFP and β-integrin at the myotendinous junction (D) Left, the dorsal ends of the LT muscles in a stage 15 *Drosophila* embryo from a time-lapse acquisition. Myonuclei, green; Aplip1–eGFP (magenta). Scale bar: 5 µm. Right, montage of a higher magnification view of Aplip1–eGFP signal (gray) from the boxed region in the left image. Arrow indicates a dynamic puncta of Aplip1–eGFP that extends from the apparent smooth muscle end (outlined with dotted line) and then moves back. Scale bar: 2 µm.

Journal of Cell Science (2018) 131, jcs205807. doi:10.1242/jcs.205807

puncta at the MTJ that were dynamic (Fig. 1D; Movie 1). Specifically, Aplip1–eGFP puncta extended away from the main cell body and back. These extensions suggest that, at late embryonic stages, after the MTJ has matured, the muscle continues to send dynamic projections and that Aplip1 is one protein component of these projections.

Aplip1 is required for muscle stability

During muscle development, filopodia-like structures extend from the muscle cell and are essential to the establishment of the cell–cell attachment that is the MTJ. A rigid structure is then built and the MTJ matures to transmit force from the muscle to the skeleton and maintain muscle integrity during contraction (Weitkunat et al., 2014). Because Aplip1–eGFP localized to MTJs, we tested whether Aplip1 contributed to muscle stability. To do this we used the *Aplip1*^{DG20707} allele that has a p-element insertion in the 3′ untranslated region (UTR) and reduced the expression of Aplip1 transcript (Fig. 2A) and counted the number of embryos that were missing lateral transverse (LT) muscles. 19.4% of control embryos were missing at least one LT muscle compared to 30% of *Aplip1*^{DG20707}/+ heterozygous embryos and 58.7% of *Aplip1*^{DG20707} homozygous embryos (Fig. 2B,D).

Missing muscles could result from either a block in the formation of the muscle during early muscle development or compromised muscle stability that causes the muscle degradation later in development. To distinguish between these possibilities, we stained late stage 16 embryos and counted the number of visibly collapsed muscles. Collapsed muscles were evident in 30% of control embryos compared to 40% of *Aplip1*^{DG20707}/+ heterozygous embryos and 60% of *Aplip1*^{DG20707} homozygous embryos (Fig. 2C,E). To support the fixed embryo data, we expressed apRed, a reporter that specifically labels the nuclei of the LT muscles (Richardson et al., 2007), and performed live-embryo time-lapse microscopy. In these movies, nuclei separated and moved toward the muscle end as has been previously described (Metzger et al., 2012; Movie 2). Often, in Aplip1 mutant embryos, after nuclei had moved toward the muscle end, one cluster of nuclei would move rapidly toward the other cluster of nuclei (Fig. 2F; Movie 3). This movement is faster than previously reported nuclear movements in muscle (Folker et al., 2014) suggesting that the movement of these nuclei is not merely irregular nuclear movement. Furthermore, clustered nuclei were never seen in a muscle with two appropriate attachments. This suggests that the muscles have detached and collapsed, and that nuclei did not move back into a cluster. Taken together, these data suggest that the missing muscles and the small muscles that are attached at only one end in the *Aplip1*^{DG20707} homozygous animals result from an inability of the muscle to form a stable MTJ.

In addition to the missing muscles and the muscles that were attached to only one end, the muscles were thinner in *Aplip1*^{DG20707} embryos. We measured the width of the LTs from the anterior edge of first LT to the posterior edge of third LT. We standardized this measure to the width of the hemisegment by dividing the width of the LTs by the width of the segment boarder. By this measure, the LT muscles in *Aplip1*^{DG20707} homozygous mutant animals were significantly thinner (Fig. 2G,H) compared to both control and *Aplip1*^{DG20707} heterozygous animals. Taken together, these data show that *Aplip1* regulates several features of muscle morphology.

Aplip1 is needed to correctly position myonuclei

Another feature of muscle development that is regulated from the muscle end is myonuclear positioning. Cytoplasmic Dynein is localized to the muscle end in a Kinesin-dependent manner. From the end of the muscle, Dynein pulls nuclei toward the muscle end (Folker et al., 2012). Because Aplip1–eGFP is localized to the muscle end and can regulate Dynein and Kinesin during axonal trafficking (Fu and Holzbaur, 2013; Horiuchi et al., 2005; Klinedinst et al., 2013; Siebert et al., 2015), we examined whether Aplip1 regulates myonuclear position. We first determined the position of nuclei in the LT muscles of stage 16 embryos as previously described (Folker et al., 2012). For these analyses, we ignored collapsed muscles and focused only on muscles that were attached at both ends. In control embryos, myonuclei were positioned in two distinct clusters adjacent to either the dorsal end of the muscle or the ventral end of the muscle as previously described (Folker et al., 2012). In *Aplip1*^{DG20707} homozygous embryos the myonuclei were significantly further from the dorsal muscle end compared to the distance in either the *Aplip1*^{DG20707} heterozygous or control embryos (Fig. 3A,B). However, the distance between the ventral end of the muscle and the nearest nucleus was the same in each genotype (Fig. 3A,C). This is likely because the myonuclei are at first clustered closer to the ventral end, and therefore the nuclei that move to the ventral end have a much shorter distance to travel. We did not see a significant difference in the LT muscle length comparing *Aplip1*^{DG20707} to controls (Fig. 3D). Thus, Aplip1 regulates myonuclear positioning in the *Drosophila* embryo.

Because Aplip1 function had been explored primarily in the nervous system, we next examined whether the effects on nuclear position were muscle autonomous. Fluorescence *in situ* hybridization demonstrated that Aplip1 is indeed expressed at low levels in the developing mesoderm (Fig. S1). Additionally, muscle specific expression of a UAS-RNAi construct that targeted Aplip1 caused an increase in the distance between either the dorsal muscle end or the ventral muscle end and the nearest nucleus without impacting muscle length (Fig. 3E–H). Taken together, these data indicate that Aplip1 functions within the muscle cell to regulate myonuclear position.

Dynamic myonuclear movement requires Aplip1

To determine the mechanism that underlies mispositioned nuclei in *Aplip1*^{DG20707} embryos, we used time-lapse microscopy to evaluate the movement of nuclei during embryonic myogenesis. As myonuclei move toward the muscle ends they develop a leading edge and a lagging edge by a Kinesin- and Dynein-dependent mechanism that is characterized by dynamic changes in the shape of nuclei (Folker et al., 2014). The average shape of nuclei [as determined by measuring the ratio of the length to the width (the aspect ratio) as described in the Materials and Methods], was the same in *Aplip1*^{DG027070} and control embryos (Fig. 4A,B). However, the myonuclei in *Aplip1*^{DG027070} embryos were less dynamic than those in controls. In control embryos, as myonuclei move toward the muscle end, they continually change between an elongated and spherical shape with aspect ratios that range from ∼3 to ∼1. However, the maximal aspect ratio of myonuclei in *Aplip1*^{DG20707} embryos is ∼2 and the minimum aspect ratio is ∼1.5 (Fig. 4A,C,D). These measurements result in a significant change in the difference between the greatest and lowest aspect ratio for each nucleus (Fig. 4E). Furthermore, nuclei exhibit fewer shape changes per hour in *Aplip1*^{DG20707} embryos compared to controls (Fig. 4F). These data suggest that *Aplip1* is needed for normal myonuclear movement during early muscle development.

Aplip1 interacts with Kinesin but not Dynein to correctly position myonuclei

To further determine the mechanism by which Aplip1 regulates myonuclear position, we evaluated genetic interactions between

Journal of Cell Science (2018) 131, jcs205807. doi:10.1242/jcs.205807

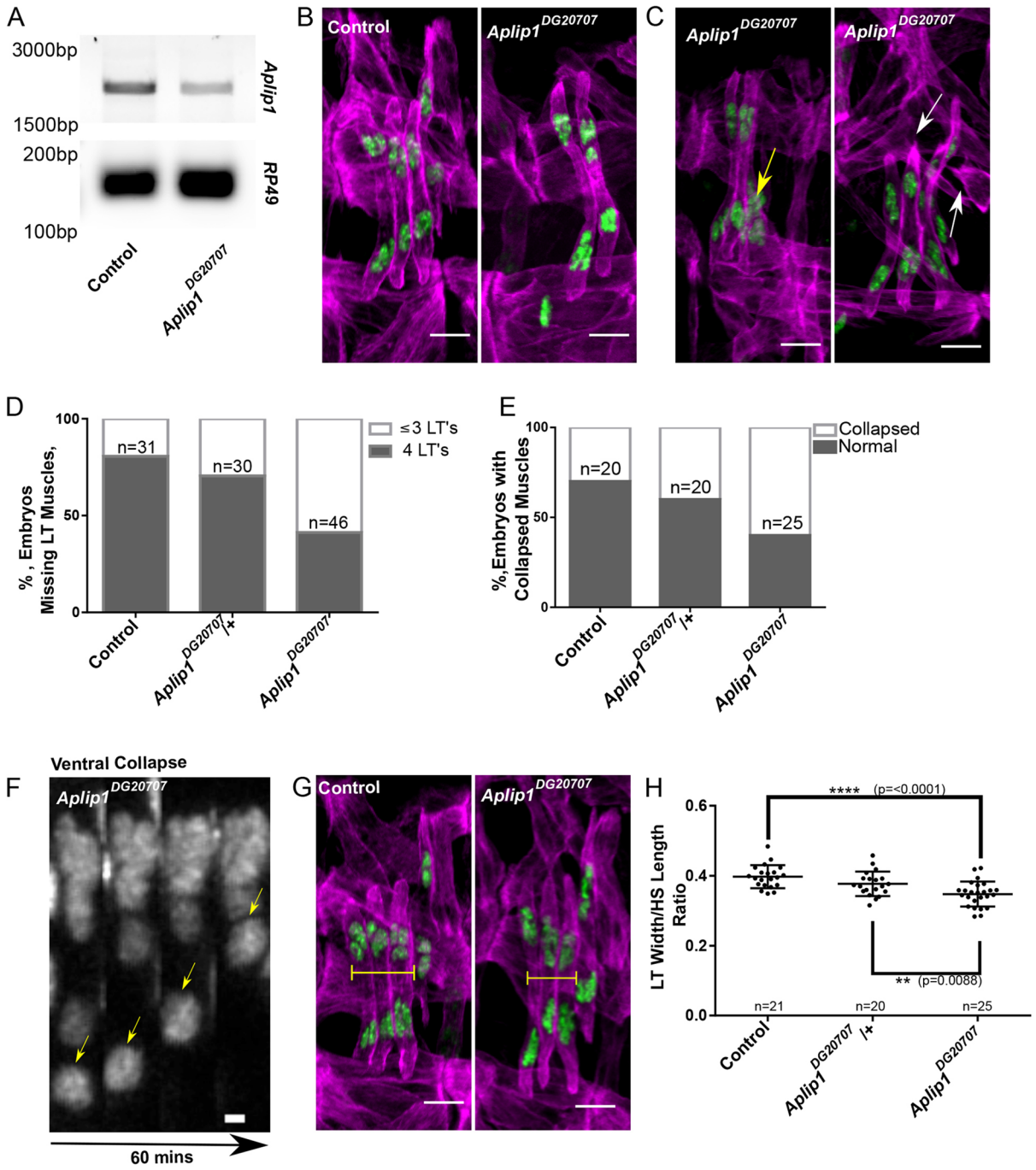

Fig. 2. *Aplip1* is required for the maintenance of muscle structure and attachments. (A) RT-PCR of *Aplip1* in control and *Aplip1*^{DG20707}, which has a P-element insertion in the 3′ UTR, flies, showing that the *Aplip1*^{DG20707} allele causes a reduction in mRNA levels. RP49 served as a control. (B) Representative immunofluorescence images of LT muscles in control and *Aplip1*^{DG20707} homozygous mutant embryos at stage 16 (16 h AEL) that show reduced muscle numbers in the *Aplip1*^{DG20707} mutants. Muscles, magenta; myonuclei, green. Scale bars: 10 µm. (C) Representative immunofluorescence images of LT muscles in control and *Aplip1* homozygous mutant embryos at stage 16 (16 h AEL). Muscles, magenta; myonuclei, green. Yellow arrows indicate collapsed LT muscles and white arrows indicate collapsed muscles that are not LTs. Scale bars: 10 µm. (D) Graph indicating that the percentage of embryos with <4 LTs is increased in *Aplip1* homozygous (*Aplip1*^{DG20707}) mutant animals compared to controls and heterozygotes. ≥30 embryos counted from at least two independent experiments. (E) Graph indicating that the percentage of visibly collapsed muscles is increased in *Aplip1* homozygous mutant animals compared to controls and heterozygotes. ≥20 embryos counted from at least two independent experiments. (F) Montage of stills from a 60 min time-lapse acquisition showing myonuclei that collapse into a single cluster following separation. In this case, the ventral cluster moved toward the dorsal cluster (arrows), but dorsal to ventral movement was equally prevalent. This phenotype was common in *Aplip1*^{DG20707} mutants, but seen rarely in controls. Scale bar: 2 µm. (G) Immunofluorescence images of LT muscles in stage 16 embryos (16 h AEL). Muscles, magenta; myonuclei, green. Yellow capped lines indicate the distance from the anterior edge of LT1 to the posterior edge of LT3. Scale bars: 10 µm. (H) Graph showing that the distance from the anterior edge of LT1 to the posterior edge of LT3 is decreased in *Aplip1* homozygous (*Aplip1*^{DG20707}) mutant animals compared to control and *Aplip1* heterozygotes (*Aplip1*^{DG20707}/+) embryos. All distances were normalized to the hemi-segment (HS) width. *n* values indicate the number of embryos examined; in each embryo at least eight muscles were analyzed and averaged. Error bars indicate s.d. from ≥20 embryos from at least two independent experiments. ***P*<0.01, *****P*<0.0001 (Student's *t*-test for comparison to controls).

Journal of Cell Science (2018) 131, jcs205807. doi:10.1242/jcs.205807

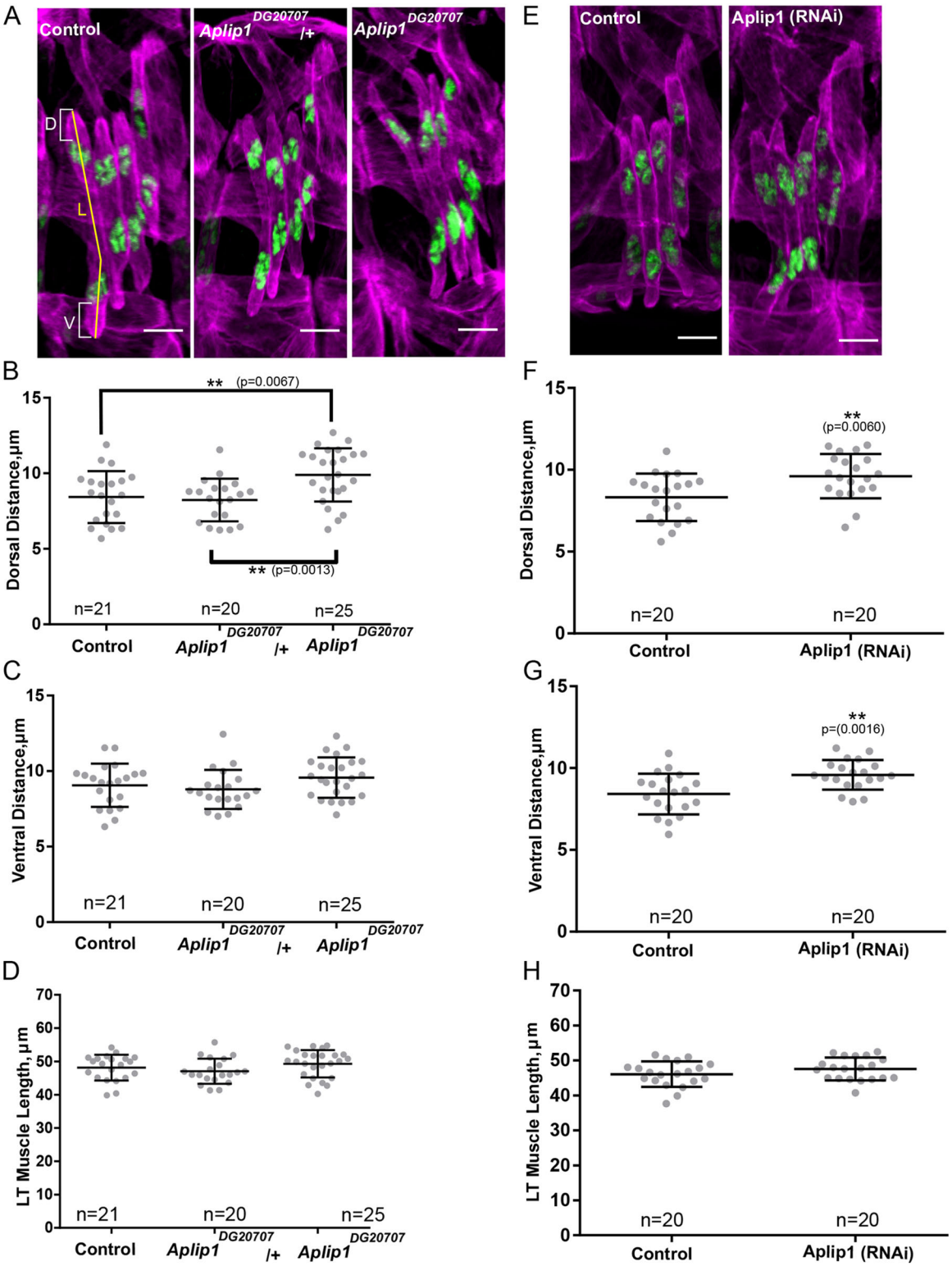

Fig. 3. Aplip1 is necessary for proper myonuclear positioning. (A) Immunofluorescence images of LT muscles in stage 16 embryos (16 h AEL) of indicated genotypes. Muscles, magenta; myonuclei, green. Brackets indicate the dorsal distance to the nearest nucleus (D) and ventral distance (V) to the nearest nucleus. The yellow line indicates the muscle length (L). (B,C) Graphs showing that the distance between the dorsal end of the muscle and the nearest nucleus was increased in the *Aplip1* homozygous mutant (*Aplip1*^{DG20707}) (B) but that the distance from the ventral end of the muscle to the closest nucleus was not affected (C) relative to controls and heterozygous embryos. (D) Graph showing that muscle length was not affected in *Aplip1* (*Aplip1*^{DG20707}) mutant embryos. (E) Immunofluorescence images of LT muscles in stage 16 embryos (16 h AEL) of indicated genotypes. Muscles, magenta; myonuclei, green. (F,G) Graphs showing that the distance between the dorsal end (F) and the ventral end (G) of the muscle and the nearest nucleus was increased when Aplip1 RNAi was expressed only in the muscle. (H) Graph showing that muscle length was not affected when Aplip1 RNAi was expressed only in the muscle. Error bars indicate s.d. from ≥20 embryos from at least two independent experiments. *n* values indicate the number of embryos that were analyzed, with at least eight muscles analyzed in each embryo. ***P*<0.01 (Student's *t*-test was for comparison to controls). Scale bars: 10 µm (A,E).

Journal of Cell Science (2018) 131, jcs205807. doi:10.1242/jcs.205807

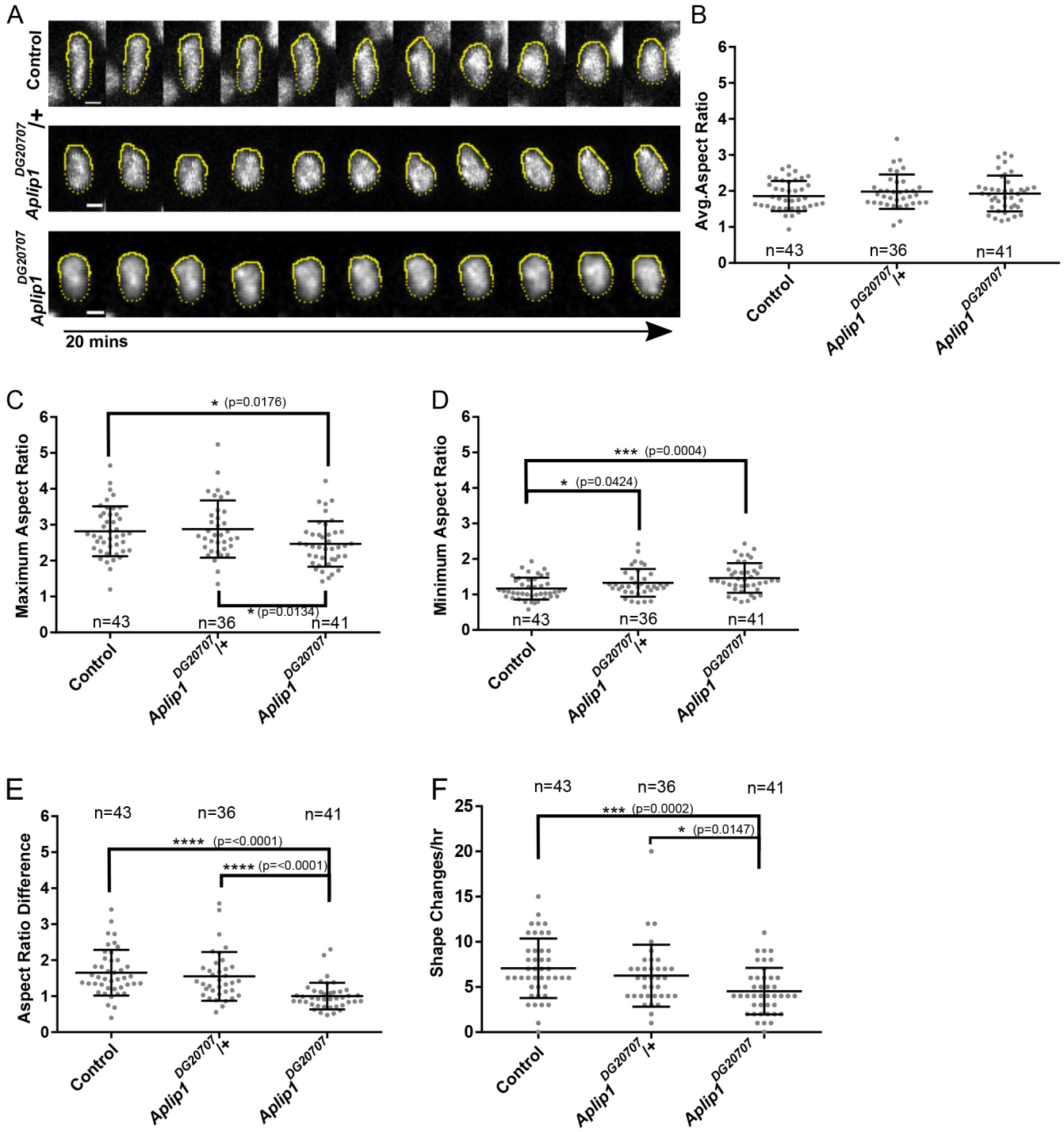

Fig. 4. Myonuclear shape changes require *Aplip1*. (A) Montage of individual myonuclei from the indicated genotypes over a 20 min time-lapse acquisition. A yellow solid line indicates the leading edge of a moving nucleus and the dotted yellow line indicates the lagging edge and completes the shape of the nucleus. Scale bars: 2 µm. (B–F) Quantification of myonuclear dynamics showing that although the average aspect ratio of myonuclei across indicated genotypes did not significantly change (B), in *Aplip1* homozygous mutant (*Aplip1*^{DG20707}) animals the nuclei were less dynamic with a lower maximum aspect ratio (less elongated) (C) and a higher minimum aspect ratio (less round) (D), which resulted in nuclei with a lower difference in maximum–minimum aspect ratio (E) and fewer shape changes (F) during a 1 h time-lapse acquisition. *n* values indicate the number of nuclei measured. Error bars indicate s.d. from ≥36 nuclei from ≥7 time-lapse acquisitions and at least three independent experiments. **P*<0.05, ****P*<0.001, *****P*<0.0001 (Student's *t*-test was used for comparison to controls).

Aplip1 and known regulators of myonuclear movement. Because Aplip1 regulates both Kinesin and Dynein during axonal transport in neurons (Fu and Holzbaur, 2013; Horiuchi et al., 2005; Klinedinst et al., 2013; Siebert et al., 2015), we first tested whether *Aplip1* interacted with either motor. To do this we carried out double heterozygous experiments using the *Aplip1*^{DG20707} allele described above, a Kinesin heavy chain null mutant (*Khc*^{8}) and a Dynein heavy chain null mutant (*Dhc64C*$^{4\text{-}19}$). The myonuclei in doubly heterozygous *Khc*^{8}/+; +/*Aplip1*^{DG20707} embryos were significantly further from both the dorsal (Fig. 5A,C) and ventral

Journal of Cell Science (2018) 131, jcs205807. doi:10.1242/jcs.205807

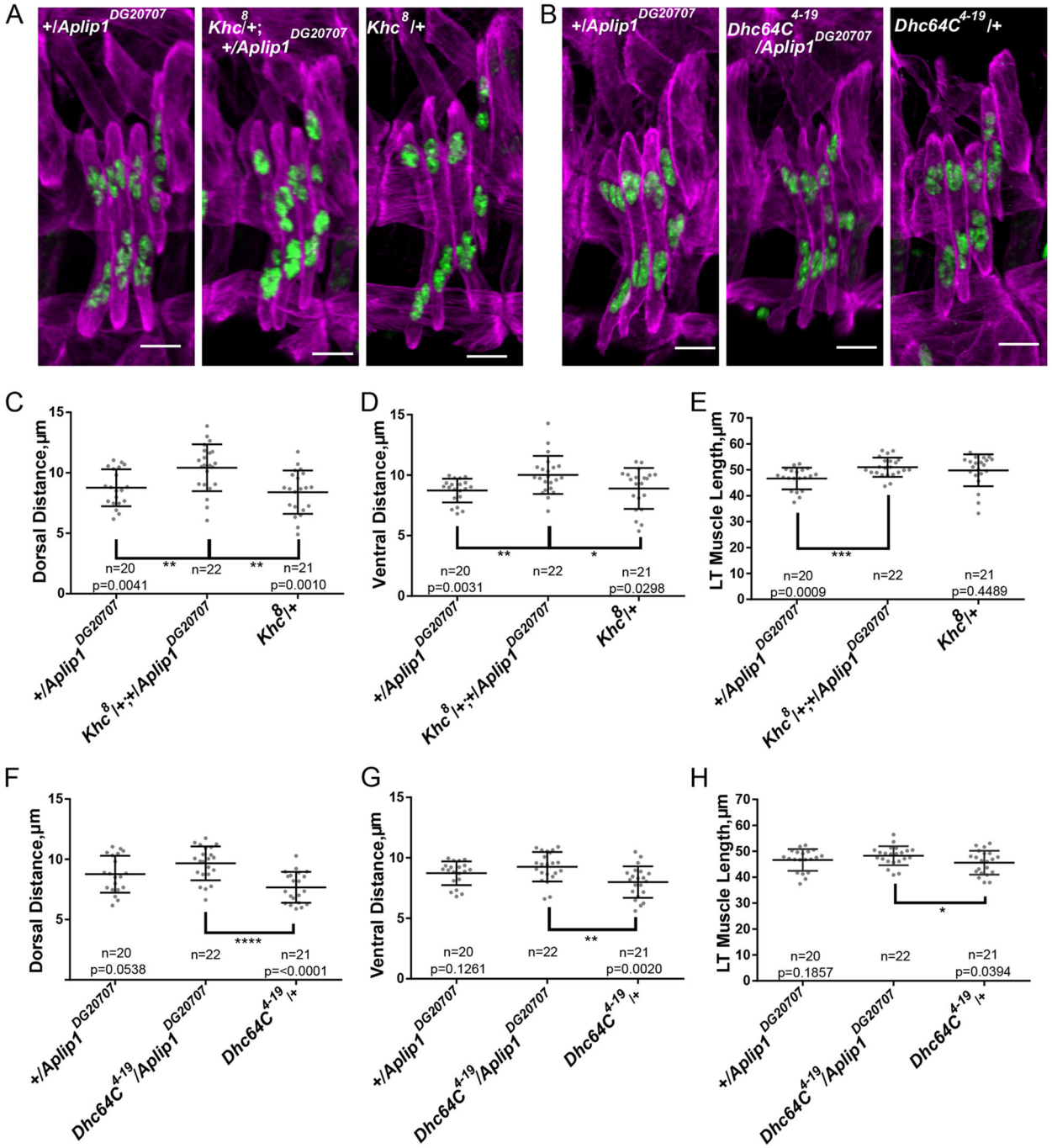

Fig. 5. *Aplip1* interacts with Kinesin but not Dynein to position myonuclei. (A) Representative immunofluorescence images of LT muscles in an *Aplip1* heterozygous mutant embryo (+/*Aplip1*^{DG20707}), Kinesin and *Aplip1* doubly heterozygous mutant embryo (*Khc*^{8}/+; +/*Aplip1*^{DG20707}), and a Kinesin heterozygous mutant embryo (*Khc*^{8}/+) at stage 16 (16 h AEL). Muscles, magenta; myonuclei, green. Scale bars: 10 µm. (B) Representative immunofluorescence images of LT muscles in an *Aplip1* heterozygous mutant embryo (+/*Aplip1*^{DG20707}), a *Dhc64C* and *Aplip1* doubly heterozygous mutant embryo (*Dhc64C*$^{4-19}$/*Aplip1*^{DG20707}), and a *Dhc64C* heterozygous mutant embryo (*Dhc64C*$^{4-19}$/+) at stage 16 (16 h AEL). Muscles, magenta; myonuclei, green. Scale bars: 10 µm. (C,D) Graphs showing that the distance from the dorsal muscle end (C) or the ventral muscle end (D) to the nearest nucleus is significantly increased in the doubly heterozygous mutants (*Khc*^{8}/+; +/*Aplip1*^{DG20707}) when compared to either *Aplip1* heterozygous mutants (+/*Aplip1*^{DG20707}) or *Khc* heterozygous mutants (*Khc*^{8}/+). (E) Graph showing that although there is a significant difference in LT muscle length between *Aplip1* heterozygous mutant embryos (+/*Aplip1*^{DG20707}) and double heterozygous embryos (*Khc*^{8}/+; +/*Aplip1*^{DG20707}), there is no difference between Kinesin heterozygous mutant embryos (*Khc*^{8}/+) and the double heterozygous embryos, indicating no genetic interaction in controlling LT muscle length. (F,G) Graphs showing that the distance from the dorsal muscle end (F) or the ventral muscle end (G) to the nearest nucleus is significantly increased in the doubly heterozygous mutants (*Dhc64C*$^{4-19}$/*Aplip1*^{DG20707}) when compared to the heterozygous mutants (*Dhc64C*$^{4-19}$/+), but not when compared to the *Aplip1* heterozygous mutant (+/*Aplip1*^{DG20707}) suggesting that *Aplip1* and *Dhc64C* do not interact to regulate nuclear position relative to the muscle end. (H) Graph showing that although there is a significant difference in LT muscle length between *Dhc64C* heterozygous mutant embryos (*Dhc64C*$^{4-19}$/+), and doubly heterozygous embryos (*Dhc64C*$^{4-19}$/*Aplip1*^{DG20707}), there is no difference between *Aplip1* heterozygous mutant embryos (+/*Aplip1*^{DG20707}) and the doubly heterozygous embryos, indicating no genetic interaction in controlling LT muscle length. *n* values indicate the number of embryos that were analyzed with at least eight muscles analyzed in each embryo. Error bars indicate s.d. from ≥20 embryos from at least two independent experiments. **P*<0.05, ***P*<0.01, ****P*<0.001, *****P*<0.0001 (Student's *t*-test for comparison to controls).

Journal of Cell Science (2018) 131, jcs205807. doi:10.1242/jcs.205807

(Fig. 5A,D) ends of the muscle when compared to the singly heterozygous embryos, indicating a functional interaction between *Khc* and *Aplip1* for the purpose of myonuclear positioning. However, the length of the LT muscles in the Khc^{8}/+; +/$Aplip1^{DG20707}$ doubly heterozygous embryos was similar to that in the Khc^{8}/+ heterozygous embryos indicating that *Aplip1* does not interact with *Khc* to regulate muscle length (Fig. 5E). To ensure that the nuclear positioning phenotype was not a result of nuclear collapse, we counted the number of embryos with missing LTs. In +/$Aplip1^{DG20707}$ and Khc^{8}/+ the percentage of embryos missing LTs was 24% and 12%, respectively. However, the Khc^{8}/+; +/$Aplip1^{DG20707}$ double heterozygous embryos only had 15% of embryos missing LT muscles showing that *Aplip1* does not interact with *Khc* to regulate muscle stability (Fig. S2A).

The same approach was used to determine whether *Aplip1* also genetically interacts with *Dhc64C* to regulate myonuclear positioning. The position of myonuclei in $Dhc64C^{4-19}$/$Aplip1^{DG20707}$ double heterozygotes was not significantly different from that in +/$Aplip1^{DG20707}$ heterozygous embryos at either the dorsal (Fig. 5B,F) or ventral end of the muscle (Fig. 5B,G), indicating that *Aplip1* and *Dhc64C* do not genetically interact to regulate myonuclear position. Additionally, the length of the muscles in $Dhc64C^{4-19}$/$Aplip1^{DG20707}$embryos was not significantly different from that in the +/$Aplip1^{DG20707}$ heterozygous embryos, indicating that *Aplip1* and *Dhc64C* do not interact to regulate muscle length (Fig. 5H). Finally, we looked at muscle stability and saw that 4% of $Dhc64C^{4-19}$/+ embryos, 24% of +/$Aplip1^{DG20707}$ embryos, and 29% of $Dhc64C^{4-19}$/$Aplip1^{DG20707}$ embryos had fewer than 4 LTs. This suggests that *Aplip1* and *Dhc64C* do not genetically interact to regulate muscle stability (Fig. S2B). These data suggest that *Aplip1* interacts with *Khc* but not *Dhc64C* to position myonuclei in the *Drosophila* embryo, and that Aplip1 regulates muscle length and attachment by a mechanism that is independent of both Kinesin and Dynein.

Aplip1 interacts with Raps to correctly position myonuclei and control the muscle length

The localization of Dynein to the muscle end for the purpose of myonuclear movement is Raps-dependent (Folker et al., 2012). From the muscle end, Dynein pulls on microtubules in a CLIP-190-dependent manner, to move the myonuclei toward the muscle pole (Folker et al., 2012, 2014). We used doubly heterozygous embryos to determine whether *Aplip1* interacts with *Raps* (Fig. 6A) or *CLIP-190* (Fig. 6B) for the purposes of nuclear positioning. The myonuclei were positioned further from both the dorsal end (Fig. 6C) and the ventral end (Fig. 6D) of the muscle in $Raps^{193}$/$Aplip1^{DG20707}$ compared to the distance in either +/$Aplip1^{DG20707}$ or $Raps^{193}$/+ heterozygous embryos. Furthermore, the muscles were longer in $Raps^{193}$/$Aplip1^{DG20707}$ compared to those in either +/$Aplip1^{DG20707}$ or $Raps^{193}$/+ singly heterozygous embryos (Fig. 6E). Additionally, 24% of +/$Aplip1^{DG20707}$ embryos, 14% of $Raps^{193}$/+ embryos, and 26% $Raps^{193}$/$Aplip1^{DG20707}$ had fewer than four LT muscles suggesting that *Aplip1* does not interact with *Raps* to regulate muscle attachment (Fig. S2C). These data indicate that *Aplip1* interacts with *Raps* to regulate both myonuclear position and muscle length. Similar evaluation of *CLIP-190*^{KG06490}/+; +/$Aplip1^{DG20707}$ doubly heterozygous embryos indicated that *Aplip1* and *CLIP-190* did not interact to regulate muscle length myonuclear positioning or muscle stability (Fig. 6F–H; Fig. S2D). Taken together, these data indicate that *Aplip1* interacts with *Raps* but not *CLIP-190* to regulate myonuclear position.

The distribution of Kinesin, Dynein and microtubules are all affected in Aplip1 mutant embryos

To further evaluate the mechanism of *Aplip1*-dependent myonuclear position, we examined the distribution of microtubules (Fig. 7), Dynein and Kinesin (Fig. 8) in *Aplip1* mutant embryos. We used the intensity of microtubule immunofluorescence as an indicator of microtubule density in a given region and focused on the region near the muscle end because changes in microtubule organization there were previously correlated with mispositioned nuclei (Folker et al., 2012). This analysis showed an increase in microtubule abundance near the muscle end in *Aplip1* mutant embryos compared to the distance in controls (Fig. 7A–C).

Similarly, mispositioned nuclei were correlated with decreased Dynein immunofluorescence at the muscle end (Folker et al., 2012) and decreased Kinesin immunofluorescence intensity near the nuclei (Folker et al., 2014). We measured the intensity of Dynein and Kinesin immunofluorescence intensity near both the nuclei and near the muscle end. The levels of Dynein were reduced both near the muscle end (Fig. 8A,C) and near the nuclei (Fig. 8B,D). Kinesin levels, however, were reduced only near the muscle end (Fig. 8E,G) and not near the nuclei (Fig. 8F,H). These data suggest that mispositioned nuclei in *Aplip1* mutants are based in changes in the organization of the microtubule network and in the distribution of microtubule motors.

DISCUSSION

Pervious work suggested that two separate pools of Kinesin and Dynein work together to move myonuclei during muscle development in *Drosophila*. One pool of the two motors exerts force directly on the nuclei (proximal pathway) (Folker et al., 2014) and the other pool pulls on nuclei from the muscle end via microtubules (cortical pathway). Kinesin-dependent transport of Dynein to the muscle end is regulated by the JNK-interacting protein (JIP) Sunday Driver (Syd, the *Drosophila* JIP3 homolog) (Schulman et al., 2014). However, beyond the role of Syd, the mechanisms by which these spatially distinct pools of Kinesin and Dynein are specified and regulated are not known. Here, we show a role for the other JIP, Aplip1, in regulating myonuclear position, myonuclear dynamics and muscle integrity.

Exogenously expressed Aplip1–eGFP localized to the muscle end (Fig. 1). This localization suggested that Aplip1 may regulate Dynein-mediated pulling forces generated from the muscle end (Folker et al., 2012). In the cortical pathway, it is thought that Dynein is transported to the muscle end by Kinesin and anchored to the cell cortex by Raps. The anchored Dynein then pulls microtubule minus-ends that are attached to the myonuclear envelope toward the muscle end (Fig. S3). Aplip1 genetically interacts with Kinesin and Raps to position myonuclei but does not genetically interact with Dynein (Figs 5 and 6). One interpretation of these data is that Aplip1 specifically regulates the ability of Dynein to pull on microtubules. Under this mechanism, Aplip1 would interact with any gene that reduced the amount of Dynein at the muscle end, known functions of *Khc* and *Raps* (Folker et al., 2012). This also suggests that sufficient Dynein is localized to the muscle end in $Dhc64C^{4-19}$/+ heterozygotes, a suggestion that is consistent with the lack of phenotype in those embryos.

The genetic interaction between *Aplip1* and *Raps*, and the strong localization of Aplip1–eGFP to the muscle end, suggest that Aplip1 functions within the cortical pathway (Fig. S3). But, Aplip1 also genetically interacted with *Khc* to position myonuclei (Fig. 5). Although Aplip1/JIP1 biochemically interacts with Kinesin (Horiuchi et al., 2007), there is no evidence that Kinesin exerts

Journal of Cell Science (2018) 131, jcs205807. doi:10.1242/jcs.205807

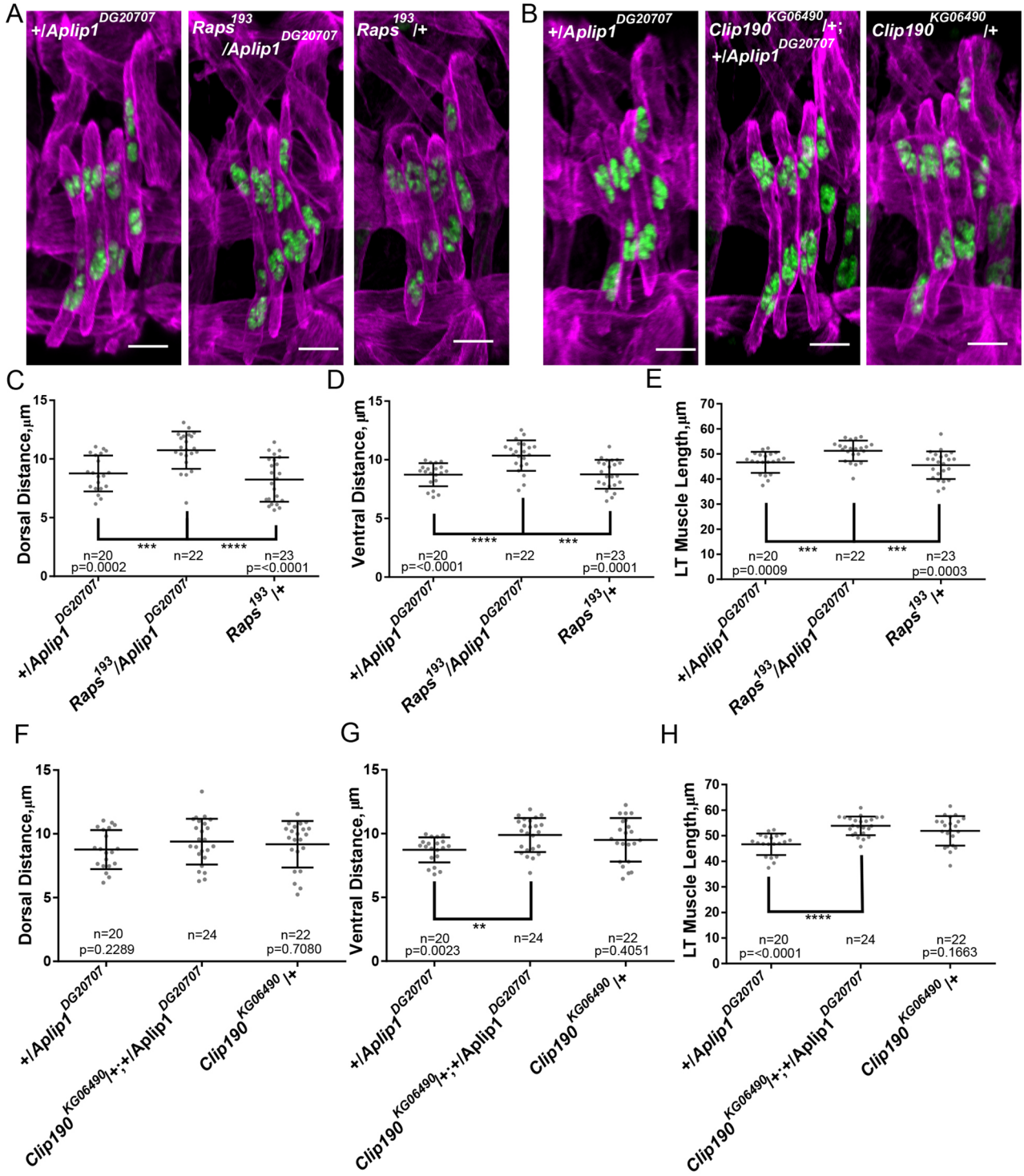

Fig. 6. *Aplip1* interacts with Raps to correctly position myonuclei and to control muscle length. (A) Representative immunofluorescence images of LT muscles in an *Aplip1* heterozygous mutant embryo (+/*Aplip1*^{DG20707}), a *Raps* and *Aplip1* doubly heterozygous mutant embryo (*Raps*^{193}/*Aplip1*^{DG20707}) and a *Raps* heterozygous mutant embryo (*Raps*^{193}/+) at stage 16 (16 h AEL). Muscles, magenta; myonuclei, green. Scale bars: 10 µm. (B) Representative immunofluorescence images of LT muscles in an *Aplip1* heterozygous mutant embryo (+/*Aplip1*^{DG20707}), a *CLIP-190* and *Aplip1* doubly heterozygous mutant embryo (*CLIP-190*^{KG06490}/+; +/*Aplip1*^{DG20707}) and a *CLIP-190* heterozygous mutant (*CLIP-190*^{KG06490}/+) at stage 16 (16 h AEL). Muscles, magenta; myonuclei, green. Scale bars: 10 µm. (C–E) Graphs showing that the distance from the dorsal muscle end (C) or the ventral muscle end (D) to the nearest nucleus is significantly increased, and that LT muscle length is also increased (E) in doubly heterozygous mutants (*Raps*^{193}/*Aplip1*^{DG20707}) when compared to either *Aplip1* heterozygous mutants (+/*Aplip1*^{DG20707}) or *Raps* heterozygous mutants (*Raps*^{193}/+). (F–H) Graphs showing that the distance from the dorsal muscle end to the nearest nucleus is not affected (F) but that the distance from the ventral muscle end to the nearest nucleus is significantly increased (G), and that LT muscle length is also increased (H) in doubly heterozygous mutants (*CLIP-190*^{KG06490}/+; +/*Aplip1*^{DG20707}) when compared to *Aplip1* heterozygous mutants (+/*Aplip1*^{DG20707}) but not when compared to *CLIP-190* heterozygous mutants (*CLIP-190*^{KG06490}/+) indicating that *CLIP-190* and *Aplip1* do not genetically interact. *n* values indicate the number of embryos that were analyzed with at least eight muscles analyzed in each embryo. Error bars indicate s.d. from ≥20 embryos from at least two independent experiments. ***P*<0.01, ****P*<0.001, *****P*<0.0001 (Student's *t*-test for comparison to controls).

Journal of Cell Science (2018) 131, jcs205807. doi:10.1242/jcs.205807

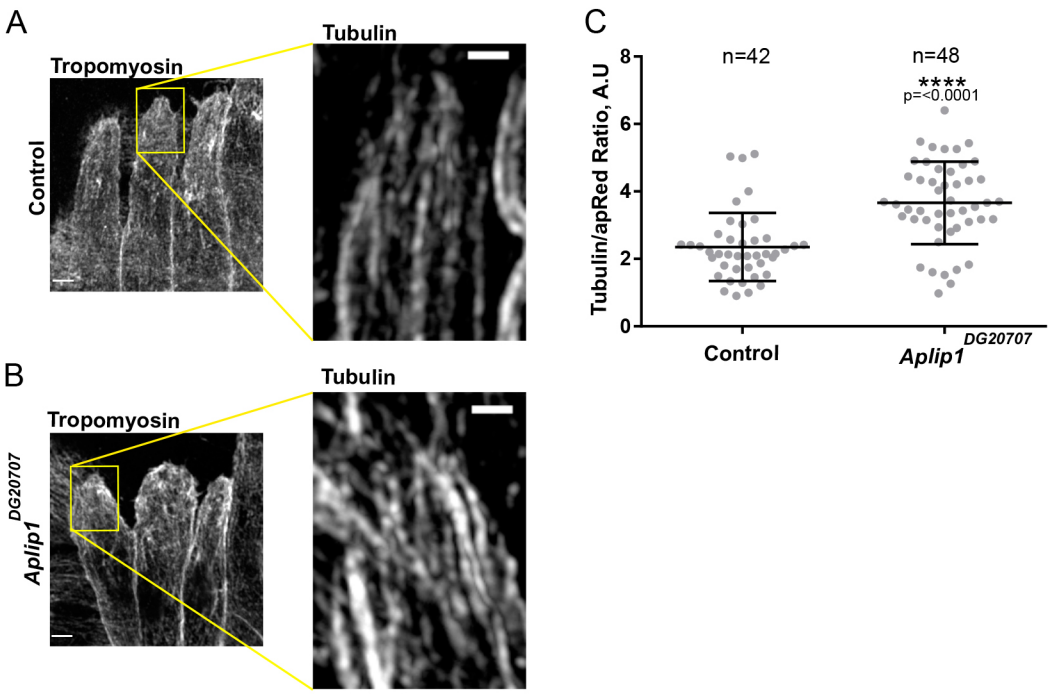

Fig. 7. Aplip1 is required for microtubule organization in muscle. (A,B) Immunofluorescence images of LT muscles (left) with the solid yellow box indicating the region of the LT muscle selected for higher magnification view (right) in control (A) and an *Aplip1*^{DG20707} mutant embryos (B). Scale bars: 1 µm (main panels); 2 µm (magnifications). (C) Graph showing that microtubule fluorescence at the muscle pole is significantly higher in *Aplip1*^{DG20707} mutant embryos when compared to controls. For each genotype, ≥42 muscles were measured from two independent experiments. Error bars indicate s.d. ****P<0.0001 (Student's t-test for comparison to controls).

force on myonuclei from the muscle end. However, we see a marked reduction in the abundance of Kinesin near the muscle end in *Aplip1* mutant embryos. This correlation may indicate that Kinesin contributes directly to the generation of force from the muscle end or may be an indication that a cargo that is transported in a Kinesin-dependent manner is essential.

Alternatively, Aplip1 may regulate Kinesin-dependent movement of nuclei in the proximal pathway. Although the Dynein–Aplip1 interaction may be promoted by JNK, the Aplip1–Kinesin interaction is inhibited by JNK activation (Horiuchi et al., 2005, 2007). This variation would allow Aplip1 to exist in two states in two distinct cellular locations for two distinct purposes. Specifically, Aplip1 near the muscle end may experience high JNK signaling that promotes interactions with Dynein whereas the Aplip1 near the cell center may experience reduced JNK signaling that promotes interactions with Kinesin.

Consistent with a role in regulating Kinesin activity within the proximal pathway, dynamic changes in nuclear shape are disrupted in *Aplip1*^{DG20707} homozygous embryos. Changes in nuclear shape are driven by the proximal pathway and are independent of the cortical pathway. In the absence of Kinesin, nuclei remain spherical and do not change shape (Folker et al., 2014). Although some changes in nuclear shape are evident in *Aplip1* mutants, they are reduced in speed and magnitude. This reduction in efficiency is consistent with Aplip1 functioning to regulate motor activity within the proximal pathway.

Beyond its contribution to myonuclear movement, Aplip1 regulates muscle width and muscle attachment. Furthermore, *Aplip1* genetically interacts with *Raps* to regulate muscle length (Fig. 6E). Increased levels of Dynein at muscle ends correlates with shorter muscles (Folker et al., 2012). However, the genetic interaction between Aplip1 and Raps results in embryos with longer muscles. This suggests that the loss of Dynein anchors (Raps) combined with reduced Aplip1 activity at the muscle end may increase Dynein retrograde movement that is correlated with increased muscle growth. More generally, these data suggest that there may be competition for Dynein between the pathways that regulate muscle length and the pathways that regulate myonuclear position.

Finally, Aplip1 regulates muscle attachment through a Kinesin- and Dynein-independent mechanism. The localization of Aplip1 to cellular extensions is similar to JIP1 localization in non-myogenic cells *in vitro* (Yasuda et al., 1999). Furthermore, the dynamic localization of Aplip1–eGFP puncta to the MTJ that seems to extend toward the tendon cell and retract back, is consistent with known mechanisms of MTJ formation (Weitkunat et al., 2014). This suggests that despite a smooth and static appearance, *Drosophila* MTJs are dynamically maintained throughout embryogenesis.

It remains unclear whether the effect on muscle structure is a result of Aplip1 playing a structural role, or if the loss of Aplip1 is contributing to a change in JNK signaling. In a dystrophic mouse muscle, overexpression of JIP1 reduced JNK signaling and improved muscle structure (Kolodziejczyk et al., 2001). Perhaps in this case, the loss of Aplip1 leads to increased activation of JNK and therefore has a detrimental effect on muscle structure.

Nevertheless, we have demonstrated that *Aplip1* is necessary for several aspects of myogenesis including MTJ development and myonuclear movement. Its ability to regulate myonuclear movement, but not MTJ development, occurs through known microtubule-dependent pathways (Klinedinst et al., 2013). Future experiments aimed at identification of the mechanism of Aplip1-dependent MTJ formation will be critical to understanding the function of Aplip1 in muscle development. More importantly, these experiments will inform potential crosstalk in the regulation of MTJ formation and myonuclear movement.

Journal of Cell Science (2018) 131, jcs205807. doi:10.1242/jcs.205807

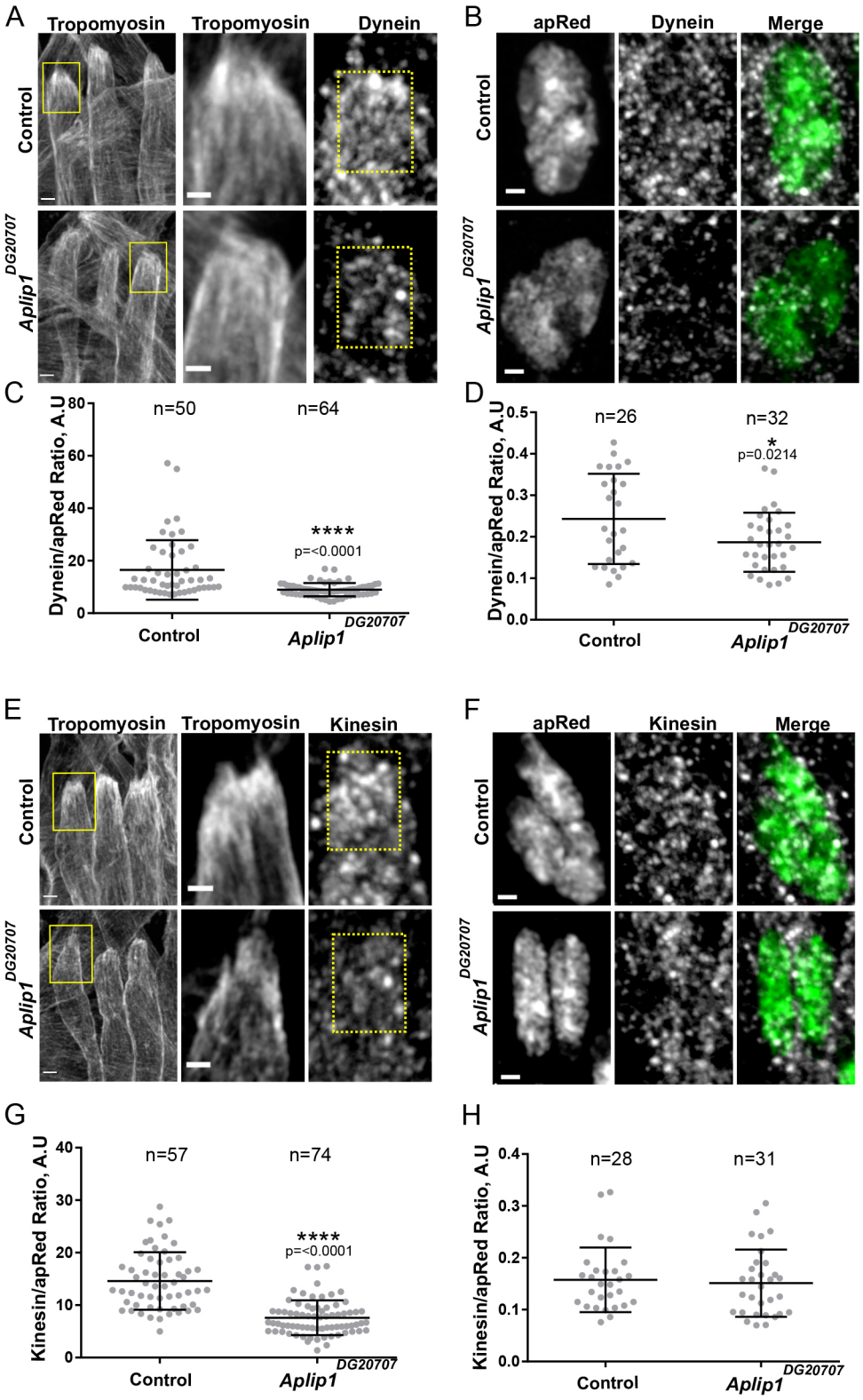

Fig. 8. Aplip1 is needed for Dynein and Kinesin localization. (A) Left, immunofluorescence images of the LT muscles of the indicated genotype with the solid yellow box indicating the area selected for higher magnification on the right. Middle, magnified image of the muscle end that was identified by immunofluorescence staining for Tropomyosin. Right, dynein signal at muscle in the magnified field indicated by the dotted yellow line that was used for analysis. Scale bars: 2 µm (left images), 1 µm (middle images). (B) Left, immunofluorescence of myonuclei from the indicated genotypes. Middle, the Dynein signal around myonuclei. Right, overlaid signals. Scale bars: 1 µm. (C,D) Graphs showing that Dynein mean fluorescence normalized to mean background fluorescence was decreased at LT muscle poles (C) and around myonuclei (D) in *Aplip1*^{DG20707} mutant embryos when compared to controls. AU, arbitrary units. (E) Left, immunofluorescence images of LT muscles of the indicated genotype, with the solid yellow box indicating the area selected for higher magnification on the right. Middle, magnified image of the muscle end identified by immunofluorescence staining for Tropomyosin. Right, Kinesin immunofluorescence in the magnified field indicated by the dotted yellow line that was used for analysis. Scale bars: 2 µm (left images), 1 µm (middle images). (F) Left, immunofluorescence of myonuclei from the indicated genotypes. Middle, the Kinesin signal around myonuclei. Right, overlaid signals. Scale bars: 1 µm. (G,H) Graphs showing that the mean Kinesin fluorescence normalized to mean background fluorescence was decreased at LT muscle poles (G) but not around myonuclei (H) in *Aplip1*^{DG20707} mutant embryos when compared to controls. Error bars indicate s.d. For analysis at the muscle pole≥0 muscles were analyzed from at least two independent experiments. For analysis at myonuclei, ≥26 clusters of myonuclei were measured from at least two independent experiments. **P*<0.05, *****P*<0.0001 (Student's *t*-test for comparison to controls).

MATERIALS AND METHODS

Drosophila genetics

The following stocks were grown under standard conditions: apRed (*apME-NLS::DsRed*) (Richardson et al., 2007), *Aplip1*^{DG20707} [21745, Bloomington *Drosophila* Stock Center (BDSC), Bloomington, IN], *Dhc64C*$^{4-19}$ (Gepner et al., 1996), *Khc*^{8} (Brendza et al., 1999), *raps*^{193} (Parmentier et al., 2000), *CLIP-190*^{KG06490} (14493,BDSC, Bloomington, IN); UAS-Aplip1 RNAi (26024, BDSC, Bloomington, IN) and UASp-Aplip1.EGFP (24634, BDSC, Bloomington, IN). All UAS lines were driven specifically in the mesoderm by *twist-GAL4, apRed* which was made as previously described (Richardson et al., 2007). For the RNAi experiment mCherry RNAi (35785, BDSC, Bloomington, IN) was driven with *twist*-GAL4 as a control. Mutants were balanced and identified using *CyO*, *DGY* or *TM6b*, *DGY*.

In double heterozygous experiments, controls were *Aplip1*^{DG20707} males crossed with virgins that expressed apRed in a *w** genetic background. This cross was necessary to ensure that the proper genetic backgrounds were compared for all analyses. In all other cases, the singly heterozygous embryos were generated by crossing virgins of the indicated genotype with apRed male flies in a *yw* background to achieve the proper genetic background. These crosses were necessary to control for differences between the *w** background that most of the alleles were carried in and the *yw* background that *Aplip1*^{DG20707} was carried in. For Fig. 2, 3 and 4, *Aplip1*^{DG20707} virgin females were crossed with apRed male flies in the *yw* background to achieve *Aplip1*^{DG20707} heterozygous embryos that were in the same genetic background as the *Aplip1*^{DG20707} homozygotes.

RNA isolation and RT-PCR

Total RNA was extracted from 20 stage 16 embryos using TRIzol (15596026, Invitrogen). The RNA concentration was then determined by using NanoDrop2000 system (Thermo Fisher Scientific Inc.). Equivalent concentrations of RNA from control and *Aplip1*^{DG20707} were then reverse transcribed by using the SuperScript VILO cDNA synthesis kit according to the manufacturer's instructions (11754050, Invitrogen, Carlsbad, CA). The *Aplip1* primer pairs used were: Aplip1-F, 5′-CCAGCAACGTCAAGGAAATTA-3′ and Aplip1-R, 5′-TGTAGATGTCCTCGATGGGATA-3′. For a loading control, RP49 was amplified with primers RP49-F, 5′-TACAGGCCCAAGATCGTGAA-3′ and RP49-R, 5′-GGTATCGACAACAGAGTGCGTC-3′.

Immunohistochemistry

Embryos were washed in 50% bleach for 3 min to remove the chorion membrane and then washed thoroughly with water. Embryos were fixed in a 1:1 dilution of heptane and 10% formalin (Sigma, Product # HT501128). Fixation was completed for 20 min on an orbital shaker at 300 rpm. For microtubule analysis, embryos were fixed in 37% formaldehyde for 10 min. After fixation, embryos were devitellinized by vortexing for 1 min in a 1:1 solution of heptane and methanol. Embryos were stained with rat anti-tropomyosin (1:200, Abcam ab50567), dsRed (1:400, Clontech 632496), rabbit anti-GFP (1:400, Torrey Pines Biolabs, catalog # TP-401), anti-integrin βPS [1:50, Developmental Studies Hybridoma Bank (DSHB), CF.6G11], mouse anti-Kinesin (1:50, DSHB SUK4), mouse anti-Dynein (1:50, DSHB 2C11-2) and mouse anti-α-tubulin (1:100, Sigma T6199) antibodies. Secondary antibodies used were Alexa Fluor 488-conjugated donkey anti-rat-IgG (1:200, A21208), Alexa Fluor 555-conjugated donkey-anti-rabbit-IgG (1:200, A31572) and Alexa Fluor 647-conjugated donkey-anti-mouse-IgG (1:200, A31571) (all Life Technologies). Embryos were mounted in ProLong Gold (Life Technologies, P36930).

Microscope settings

For Dynein, Kinesin and microtubule imaging a Zeiss LSM 880 Airyscan with a C-Plan-APOCHROMAT 40×1.3 NA objective was used. Embryos stained for Dynein and Kinesin were imaged using the 'resolution versus sensitivity' setting due to the low signal. For microtubule staining, the superresolution setting was used. All embryos were put through manual Airyscan processing in order to compare images. For all other images, a Zeiss LSM 700 microscope using an APOCHROMAT 40×, 1.4 NA objective was used. The zoom for each experiment is stated in the relevant Materials and Methods section.

Nuclear positioning analysis

Embryos were imaged on a Zeiss LSM 700 microscope using an APOCHROMAT 40×, 1.4 NA objective with a 1.0× optical zoom. Stage 16 embryos were identified as previously described (Folker et al., 2012). The distance from the dorsal or ventral tip of the four lateral transverse (LTs) muscles to the nearest nucleus was measured by using the line tool in ImageJ (NIH). The distances between the muscle end and the nearest nucleus were averaged from all four LT muscles from between two to four hemisegments for each data point that is presented. Nuclear position was measured in at least two independent experiments that included ≥20 embryos from each genotype. The minimum *n*-value required was determined by using software at https://www.stat.ubc.ca/~rollin/stats/ssize/n2.html. Statistical analysis was completed with Prism 4.0 (GraphPad) using a Students *t*-test with <0.05 considered significant.

Muscle morphology analysis

Embryos were imaged with an APOCHROMAT 40×, 1.4 NA objective with a 1.0× optical zoom. LT muscle width was measured from the anterior edge of LT1 to the posterior edge of LT3, at the center of the muscles on the dorsal–ventral axis. This measure was normalized to the width of the hemisegment, which was measured as the distance between two myotendinous junctions (MTJs) using the line tool in ImageJ (NIH). LT width measurements were taken in at least two independent experiments that included ≥20 embryos from each genotype. Statistical analysis was completed with Prism 4.0 (GraphPad) using a Student's *t*-test with <0.05 considered significant.

For the missing LT count, each microscope slide was scanned using the Zeiss LSM 700 microscope in each respective genotype and an embryo was scored as either normal or having missing LTs. A total of ≥20 embryos were counted for each genotype. For collapsed muscle analysis images were taken with an APOCHROMAT 40×, 1.4 NA objective with a 1.0× optical zoom. An embryo was then scored as either having visibly collapsed muscles or not. For this analysis, all muscles were considered, rather than just the LT muscles. A total of ≥20 were counted for each genotype.

MTJ imaging and colocalization analysis

To measure the colocalization of Aplip1 and β-PS-integrin, Aplip1–eGFP and β-integrin were imaged in *Drosophila* embryos that expressed Aplip1–eGFP. Images were acquired on a Zeiss LSM700 microscope using an APOCHROMAT 40×, 1.4 NA objective and a step size of 0.5 µm. Images at the MTJ of the Dorsal (DO) muscles were acquired with a 2.2× optical zoom, whereas images of the LT muscle ends were acquired with a 3.6× optical zoom. For the DO2 muscle (Fig. 1B) colocalization analysis, a 5 µm line-scan was performed through the MTJ in both the β-integrin and Aplip1–eGFP channel. The raw intensity data was then overlaid from both channels.

Live imaging

Embryos were dechorionated with a 3 min incubation in 50% bleach. Embryos were then washed in water to remove all the bleach and mounted on a gas-permeable membrane with halocarbon oil (Sigma, product # H8898). Late stage 15 embryos were selected as previously described (Folker et al., 2012) and time lapse images were taken at a rate of 2 min/stack (except for Fig. 1D and Movie 1 which were taken at 10 s/stack at a zoom of 2.2×) and a step size of 1 µm for 1 h using an APOCHROMAT 40×, 1.4 NA objective with a 1.6× optical zoom on a Zeiss 700 LSM.

Nuclear aspect ratio analysis

The aspect ratio of each nucleus was determined by measuring the length of each nucleus on the dorsal-ventral axis and dividing it by the length of each nucleus on the anterior-posterior axis by using the line tool in ImageJ (NIH). A nucleus was judged to change shape if the aspect ratio changed by ≥0.5. A total of ≥36 nuclei were examined from ≥7 movies per genotype indicated and from at least three independent experiments. Statistical analysis was carried out with Prism 4.0 (GraphPad) using a Student's *t*-test with <0.05 considered significant.

Kinesin, dynein and microtubule localization measurements

Stage 16 embryos, stained with either the anti-Dynein, -Kinesin or -α-tubulin antibody, were aged as previously described (Folker et al., 2012). For Dynein, Kinesin or microtubule analysis at the muscle pole, the tropomyosin signal was used to select *Z*-stacks to ensure all of the Dynein, Kinesin or microtubule signal was fully within the muscle. Maximum projections were then made and a box of set dimensions (2×3 µm) was drawn over the end of the muscle. The mean fluorescence of Kinesin, Dynein or microtubules was measured. The value was then normalized to the background signal (immunostaining against DsRed) within the same box. A total of ≥50 muscles were examined from at least two independent experiments.

To measure Dynein and Kinesin localization near the nucleus the apRed signal was used to crop each cluster of nuclei from the top to the bottom. Z-stacks were then converted into maximum intensity projections. The mean fluorescence of Dynein or Kinesin was then measured around each nuclear cluster and normalized to the mean apRed fluorescence. These measurements were taken using a custom MATLAB program based on the image segmentation tool (MathWorks), which can be obtained from the author upon request. Briefly, using the apRed channel the perimeter of each cluster of nuclei was established and the mean apRed fluorescence was measured from inside this area. Based on where the coordinate of points in the perimeter were located with respect to the center of the nucleus, the perimeter was expanded outward by 5 pixels. It was from this expanded area that the mean fluorescence of Kinesin or Dynein was taken. A total of ≥26 clusters of nuclei were examined from at least two independent experiments.

Dynein, Kinesin and microtubules were imaged using the Zeiss LSM 880 Airyscan with a C-Plan-APOCHROMAT 40×1.3 NA objective. Dynein images were taken at a zoom of 5×, Kinesin images were taken at a zoom of 6× and microtubule images were taken at a zoom of 7.2×. Statistical analysis was carried out with Prism 4.0 (GraphPad) using a Student's *t*-test, with <0.05 considered significant.

Fluorescence *in situ* hybridization

RNA fluorescence *in situ* hybridization (FISH) was carried out as previously described (Legendre et al., 2013). Briefly, cDNA was made as described above from stage 16 embryos. Antisense and sense (used as a negative control) probes of Aplip1 were created by using T7 polymerase (FEREP0111, Fisher) and labeled with DIG-UTP nucleotide mix (11209256910, Sigma). Embryos were fixed as described above and each probe was hybridized for 14 h. Post hybridization the probe was detected using a biotin-conjugated mouse anti-DIG (200-062-156, Jackson ImmunoResearch) and streptavidin-conjugated horseradish peroxidase (HRP; S911A, Fisher). To enable fluorescence, a cyanine 3 tyramide reagent kit was used (SAT704A001EA, Perkin Elmer).

Acknowledgements

We thank the Bret Judson and the Boston College Imaging Core for infrastructure and support. Additionally, Casey Kraft from Carl Zeiss Microscpy, LLC provided critical support in performing localization studies using the Zeiss AiryScan microscope. *Drosophila* stocks obtained from the Bloomington Drosophila Stock Center (NIHP400D018537) were used in this study. The integrin betaPS antibody developed by D. Brower at Harvard Medical School was obtained from the Developmental Studies Hybridoma Bank, created by the NICHD of the NIH and maintained at the University of Iowa, Department of Biology, Iowa City, IA 52242.

Competing interests

The authors declare no competing or financial interests.

Author contributions

Conceptualization: E.S.F.; Methodology: A.L.A., S.A.R., E.S.F.; Software: S.A.R.; Formal analysis: A.L.A., S.A.R., C.B.M., J.M.C.; Investigation: A.L.A., C.B.M., J.M.C.; Resources: E.S.F.; Writing - original draft: A.L.A.; Writing - review & editing: A.L.A., E.S.F.; Visualization: A.L.A.; Supervision: E.S.F.; Project administration: E.S.F.; Funding acquisition: E.S.F.

Funding

This work was supported by grants from the American Heart Association to E.S.F. (15SDG22460004) as well as funds from Boston College.

Supplementary information

Supplementary information available online at
http://jcs.biologists.org/lookup/doi/10.1242/jcs.205807.supplemental

References

Bao, Z. Z., Lakonishok, M., Kaufman, S. and Horwitz, A. F. (1993). Alpha 7 beta 1 integrin is a component of the myotendinous junction on skeletal muscle. *J. Cell Sci.* **106**, 579-589.

Brendza, K. M., Rose, D. J., Gilbert, S. P. and Saxton, W. M. (1999). Lethal kinesin mutations reveal amino acids important for ATPase activation and structural coupling. *J. Biol. Chem.* **274**, 31506-31514.

Bruusgaard, J. C., Liestøl, K. and Gundersen, K. (2006). Distribution of myonuclei and microtubules in live muscle fibers of young, middle-aged, and old mice. *J. Appl. Physiol.* **100**, 2024-2030.

Cadot, B., Gache, V., Vasyutina, E., Falcone, S., Birchmeier, C. and Gomes, E. R. (2012). Nuclear movement during myotube formation is microtubule and dynein dependent and is regulated by Cdc42, Par6 and Par3. *EMBO Rep.* **13**, 741-749.

Cavalli, V., Kujala, P., Klumperman, J. and Goldstein, L. S. B. (2005). Sunday Driver links axonal transport to damage signaling. *J. Cell Biol.* **168**, 775-787.

Folker, E. S., Schulman, V. K. and Baylies, M. K. (2012). Muscle length and myonuclear position are independently regulated by distinct Dynein pathways. *Development* **139**, 3827-3837.

Folker, E. S., Schulman, V. K. and Baylies, M. K. (2014). Translocating myonuclei have distinct leading and lagging edges that require kinesin and dynein. *Development* **141**, 355-366.

Fu, M.-M. and Holzbaur, E. L. F. (2013). JIP1 regulates the directionality of APP axonal transport by coordinating kinesin and dynein motors. *J. Cell Biol.* **202**, 495-508.

Gepner, J., Li, M., Ludmann, S., Kortas, C., Boylan, K., Iyadurai, S. J., McGrail, M. and Hays, T. S. (1996). Cytoplasmic dynein function is essential in Drosophila melanogaster. *Genetics* **142**, 865-878.

Greig, S. and Akam, M. (1993). Homeotic genes autonomously specify one aspect of pattern in the Drosophila mesoderm. *Nature* **362**, 630-632.

Horiuchi, D., Barkus, R. V., Pilling, A. D., Gassman, A. and Saxton, W. M. (2005). APLIP1, a kinesin binding JIP-1/JNK scaffold protein, influences the axonal transport of both vesicles and mitochondria in drosophila. *Curr. Biol.* **15**, 2137–2141.

Horiuchi, D., Collins, C. A., Bhat, P., Barkus, R. V., DiAntonio, A. and Saxton, W. M. (2007). Control of a kinesin-cargo linkage mechanism by JNK pathway kinases. *Curr. Biol.* **17**, 1313-1317.

Iyer, S. R., Shah, S. B., Valencia, A. P., Schneider, M. F., Hernandez-Ochoa, E. O., Stains, J. P., Blemker, S. S. and Lovering, R. M. (2017). Altered nuclear dynamics in MDX myofibers. *J. Appl. Physiol.* **122**, 470-481.

Jeannet, P.-Y., Bassez, G., Eymard, B., Laforet, P., Urtizberea, J. A., Rouche, A., Guicheney, P., Fardeau, M. and Romero, N. B. (2004). Clinical and histologic findings in autosomal centronuclear myopathy. *Neurology* **62**, 1484-1490.

Klinedinst, S., Wang, X., Xiong, X., Haenfler, J. M. and Collins, C. A. (2013). Independent pathways downstream of the Wnd/DLK MAPKKK regulate synaptic structure, axonal transport, and injury signaling. *J. Neurosci.* **33**, 12764-12778.

Kolodziejczyk, S. M., Walsh, G. S., Balazsi, K., Seale, P., Sandoz, J., Hierlihy, A. M., Rudnicki, M. A., Chamberlain, J. S., Miller, F. D. and Megeney, L. A. (2001). Activation of JNK1 contributes to dystrophic muscle pathogenesis. *Curr. Biol.* **11**, 1278-1282.

Legendre, F., Cody, N., Iampietro, C., Bergalet, J., Lefebvre, F. A., Moquin-Beaudry, G., Zhang, O., Wang, X. and Lécuyer, E. (2013). Whole mount RNA fluorescent in situ hybridization of Drosophila embryos. *J. Vis. Exp.* **71**, e50057.

Meinke, P., Mattioli, E., Haque, F., Antoku, S., Columbaro, M., Straatman, K. R., Worman, H. J., Gundersen, G. G., Lattanzi, G., Wehnert, M. et al. (2014). Muscular dystrophy-associated SUN1 and SUN2 variants disrupt nuclear-cytoskeletal connections and myonuclear organization. *PLoS Genet.* **10**, e1004605.

Metzger, T., Gache, V., Xu, M., Cadot, B., Folker, E. S., Richardson, B. E., Gomes, E. R. and Baylies, M. K. (2012). MAP and kinesin-dependent nuclear positioning is required for skeletal muscle function. *Nature* **484**, 120-124.

Parmentier, M. L., Woods, D., Greig, S., Phan, P. G., Radovic, A., Bryant, P. and O'Kane, C. J. (2000). Rapsynoid/partner of inscuteable controls asymmetric division of larval neuroblasts in Drosophila. *J. Neurosci.* **20**, RC84.

Pines, M., Das, R., Ellis, S. J., Morin, A., Czerniecki, S., Yuan, L., Klose, M., Coombs, D. and Tanentzapf, G. (2012). Mechanical force regulates integrin turnover in Drosophila in vivo. *Nat. Cell Biol.* **14**, 935-943.

Rai, M., Nongthomba, U. and Grounds, M. D. (2014). Skeletal muscle degeneration and regeneration in mice and flies. In *Current Topics in Developmental Biology*, *Mechanisms of Regeneration* (Ed: B. Galliot), pp. 247-281. Elsevier.

Richardson, B. E., Beckett, K., Nowak, S. J. and Baylies, M. K. (2007). SCAR/WAVE and Arp2/3 are crucial for cytoskeletal remodeling at the site of myoblast fusion. *Development* **134**, 4357-4367.

Schulman, V. K., Folker, E. S., Rosen, J. N. and Baylies, M. K. (2014). Syd/JIP3 and JNK signaling are required for myonuclear positioning and muscle function. *PLoS Genet.* **10**, e1004880.

Siebert, M., Böhme, M. A., Driller, J. H., Babikir, H., Mampell, M. M., Rey, U., Ramesh, N., Matkovic, T., Holton, N., Reddy-Alla, S. et al. (2015). A high affinity RIM-binding protein/Aplip1 interaction prevents the formation of ectopic axonal active zones. *Elife* **4**.

Spiro, A. J., Shy, G. M. and Gonatas, N. K. (1966). Myotubular myopathy. Persistence of fetal muscle in an adolescent boy. *Arch. Neurol.* **14**, 1-14.

Taru, H., Iijima, K.-I., Hase, M., Kirino, Y., Yagi, Y. and Suzuki, T. (2002). Interaction of Alzheimer's beta -amyloid precursor family proteins with scaffold proteins of the JNK signaling cascade. *J. Biol. Chem.* **277**, 20070-20078.

van Bergeijk, P., Hoogenraad, C. C. and Kapitein, L. C. (2016). Right time, right place: probing the functions of organelle positioning. *Trends Cell Biol.* **26**, 121-134.

Volk, T., Fessler, L. I. and Fessler, J. H. (1990). A role for integrin in the formation of sarcomeric cytoarchitecture. *Cell* **63**, 525-536.

Weitkunat, M., Kaya-Çopur, A., Grill, S. W. and Schnorrer, F. (2014). Tension and force-resistant attachment are essential for myofibrillogenesis in Drosophila flight muscle. *Curr. Biol.* **24**, 705-716.

Wilson, M. H. and Holzbaur, E. L. F. (2012). Opposing microtubule motors drive robust nuclear dynamics in developing muscle cells. *J. Cell Sci.* **125**, 4158-4169.

Wilson, M. H. and Holzbaur, E. L. F. (2015). Nesprins anchor kinesin-1 motors to the nucleus to drive nuclear distribution in muscle cells. *Development* **142**, 218-228.

Yasuda, J., Whitmarsh, A. J. and Cavanagh, J., Sharma, M. and Davis, R. J. (1999). The JIP group of mitogen-activated protein kinase scaffold proteins. *Mol. Cell. Biol.* **19**, 7245-7254.

Supplementary Information

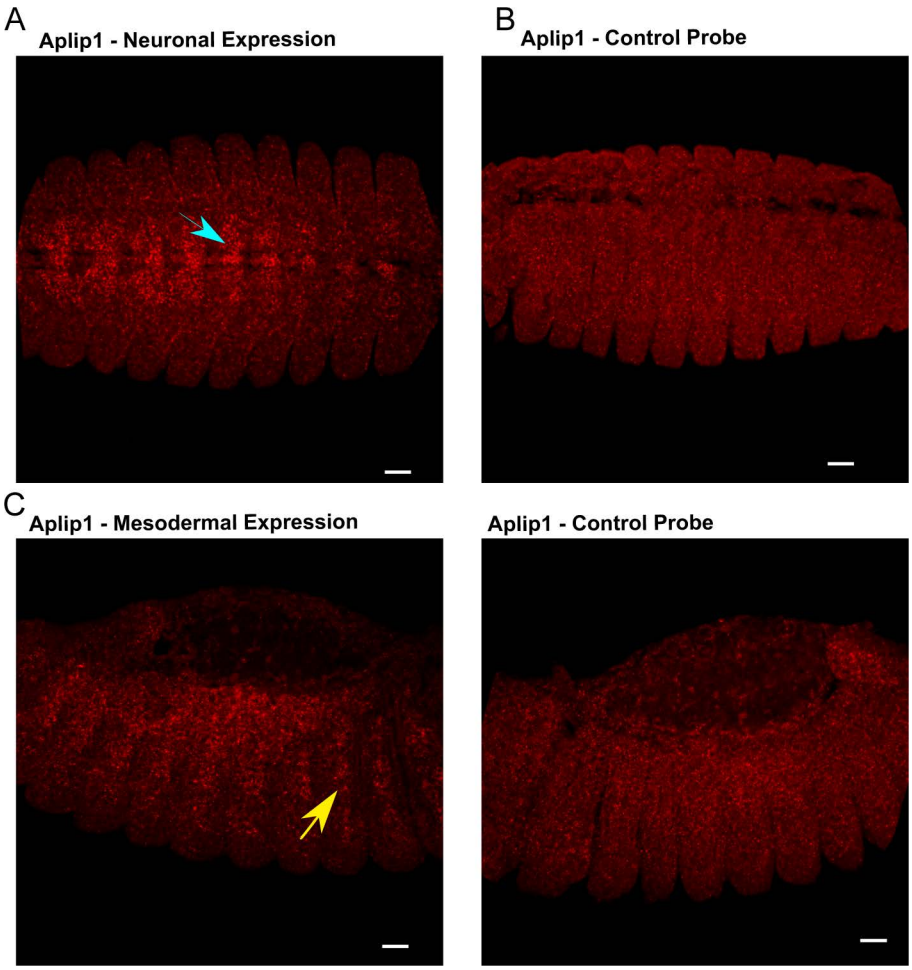

Figure S1. Fluorescent in situ hybridization (FISH) of *Aplip1* in Drosophila embyos.
A-B) Stage 13 embryo showing neuronal expression (cyan arrow) of Aplip1 using an antisense probe **(A)** or a control sense probe to indicate background signal **(B) C-D)** Stage 13 embryo showing mesodermal expression (yellow arrow) of Aplip1 using an antisense probe (Red) **(C)** or a control sense probe showing background signal **(D)**

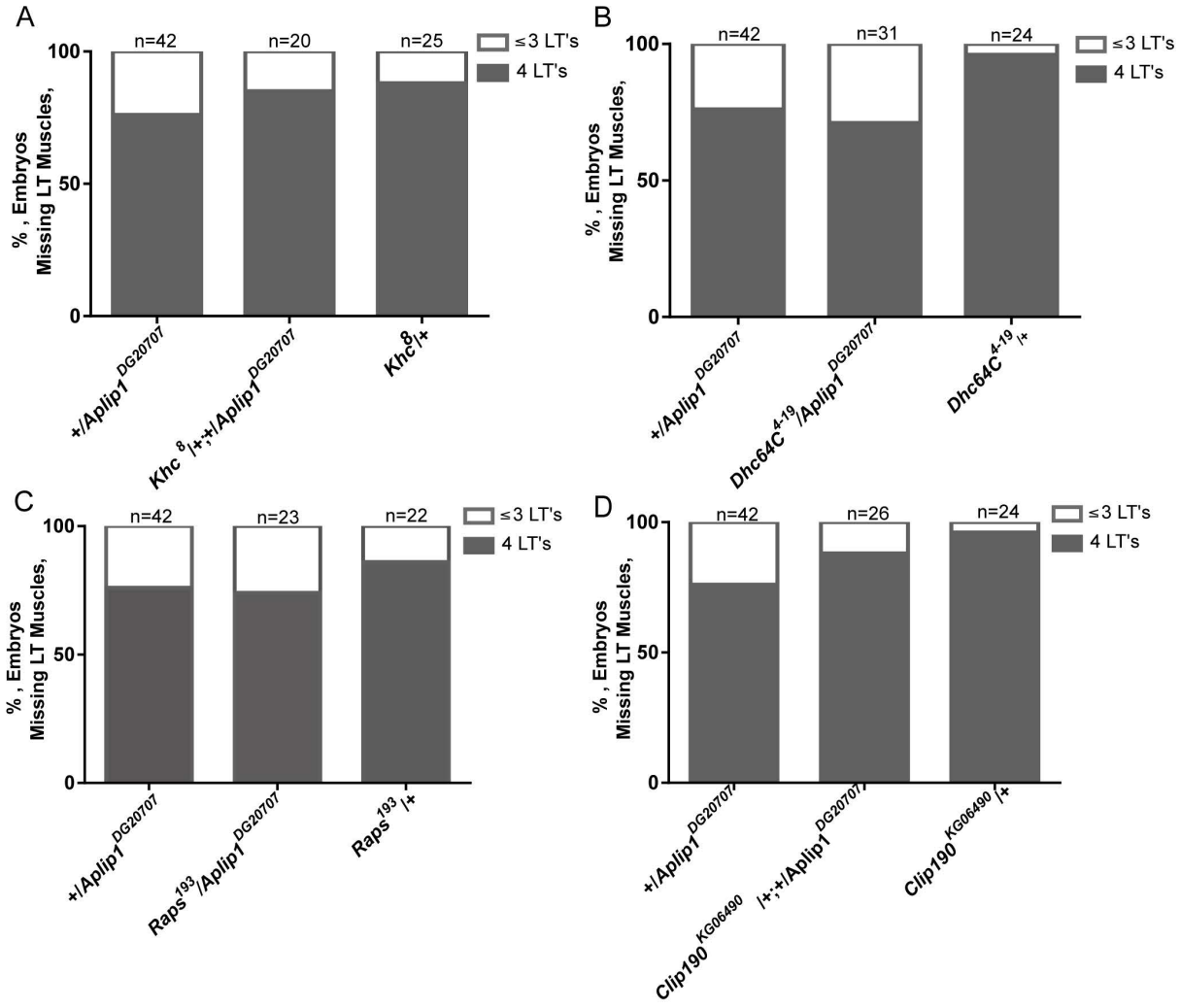

Figure S2. *Aplip1* does not interact with cytoskeletal proteins to regulate muscle stability. A-D) Graphs indicating that the percentage of embryos with < 4 LTs is not significantly different when *Aplip1* heterozygous mutants (+/*Aplip1*^{DG20707}) and *Kinesin* heterozygous mutants (*Khc*^{8}/+) are compared to *Kinesin* and *Aplip1* doubly heterozygous mutant embryos (*Khc*^{8}/+; +/*Aplip1*^{DG20707}) **(A),** *Aplip1* heterozygous mutants (+/*Aplip1*^{DG20707}) and *Dynein* heterozygous mutants (*Dhc64C*$^{4-19}$/+) compared to *Dynein* and *Aplip1* double heterozygous mutant embryo (*Dhc64C*$^{4-19}$/*Aplip1*^{DG20707}) **(B),** *Aplip1* heterozygous mutants (+/*Aplip1*^{DG20707}) and *Raps* heterozygous mutants (*Raps*^{193}/+) compared to *Raps* and *Aplip1* double heterozygous mutant embryos (*Raps*^{193}/*Aplip1*^{DG20707}) **(C)** and *Aplip1* heterozygous mutants (+/*Aplip1*^{DG20707}) and *Clip-190* heterozygous mutants (*Clip-190*^{KG06490}/+) compared to *Clip-190* and *Aplip1* double heterozygous mutant embryo (*Clip-190*^{KG06490}/+; +/*Aplip1*^{DG20707}) **(D).**

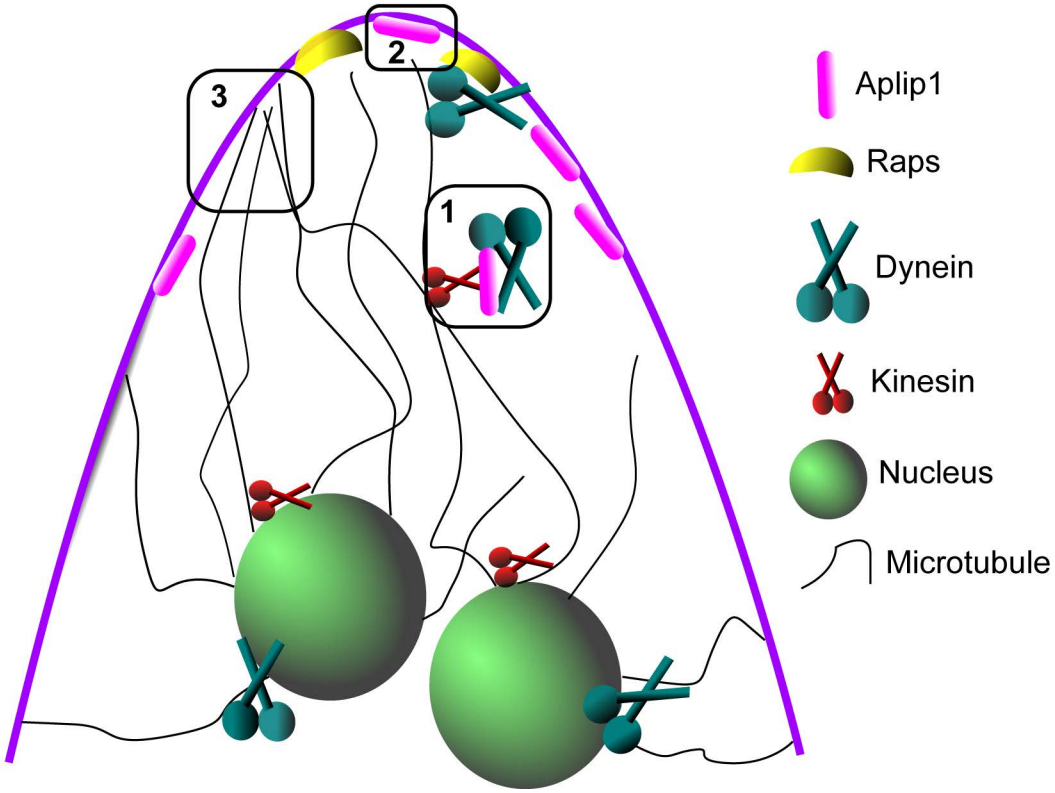

Figure S3. Model of the role of Aplip1 in myonuclear positioning and muscle stability. In Aplip1 mutant embryos there are reduced levels of both Dynein and Kinesin near the muscle ends. This suggests that one function of Aplip1 may be to regulate Kinesin-dependent transport of Dynein toward the muscle end (1). Additionally, there is a strong genetic interaction between Aplip1 and Raps, a gene previously demonstrated to be important for Dynein localization. This suggests that Aplip1 may additionally function in the anchoring and/or activation of anchored Dynein for the purpose of myonuclear movement (2). Finally, there is an increase in the abundance of MTs at the ends of muscles in Aplip1 mutants. This suggests either that there is a compensation mechanism to stabilize microtubules directed toward the muscle end or that Aplip1 directly contributes to the dynamics of microtubules near the muscle end (3).

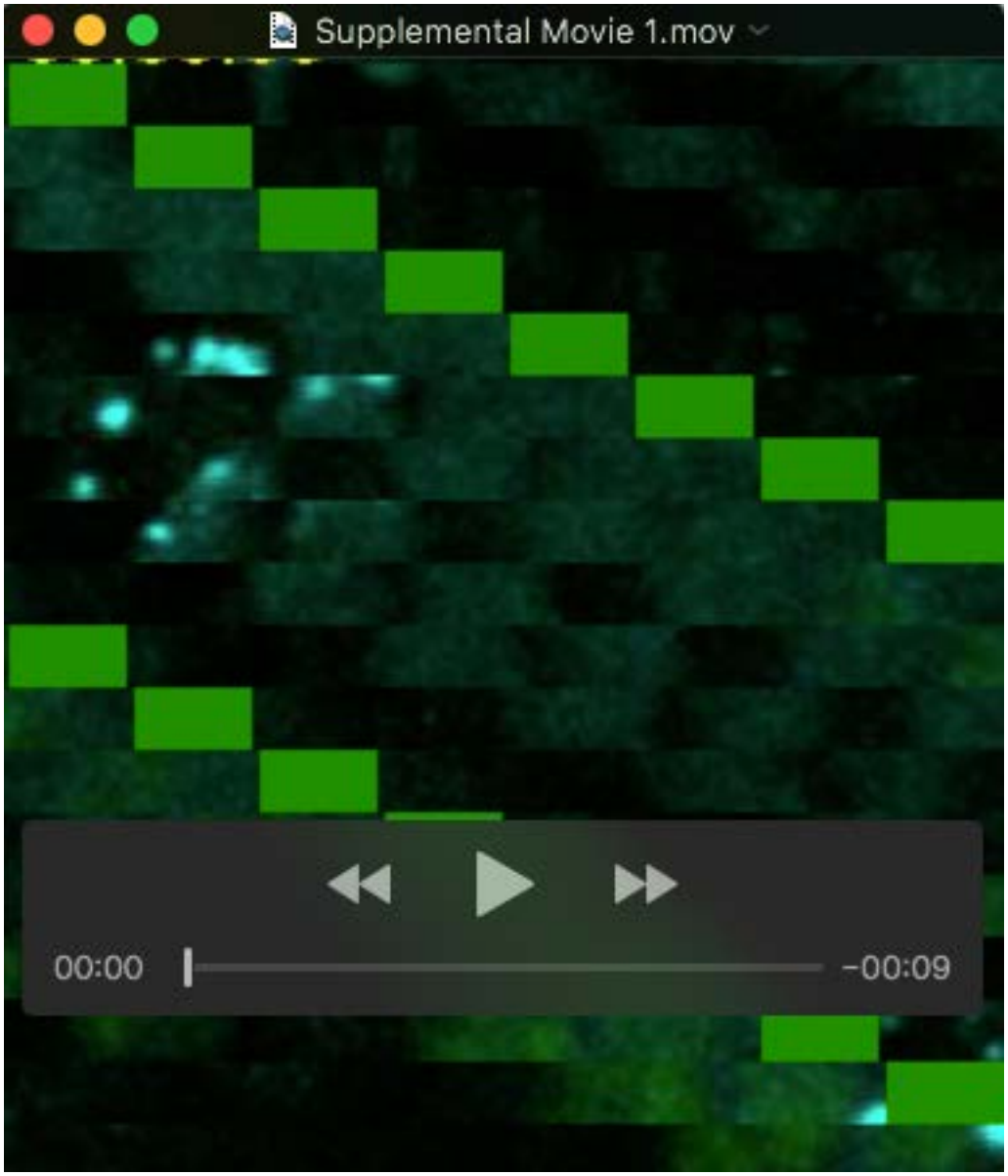

Movie S1. Aplip1eGFP dynamics at the MTJ

LT muscles of the *Drosophila* embryo expressing Aplip1-eGFP (Cyan) with nuclei (green). Aplip1-eGFP accumulates at MTJs where it forms dynamic puncta extending from the muscle pole. Time-lapse movies shown as maximum projections. Z-stacks were acquired at a rate of 1 frame/10 secs. Movie plays at 10 frames/s. Scale bar, 5 µm.

Journal of Cell Science • Supplementary information

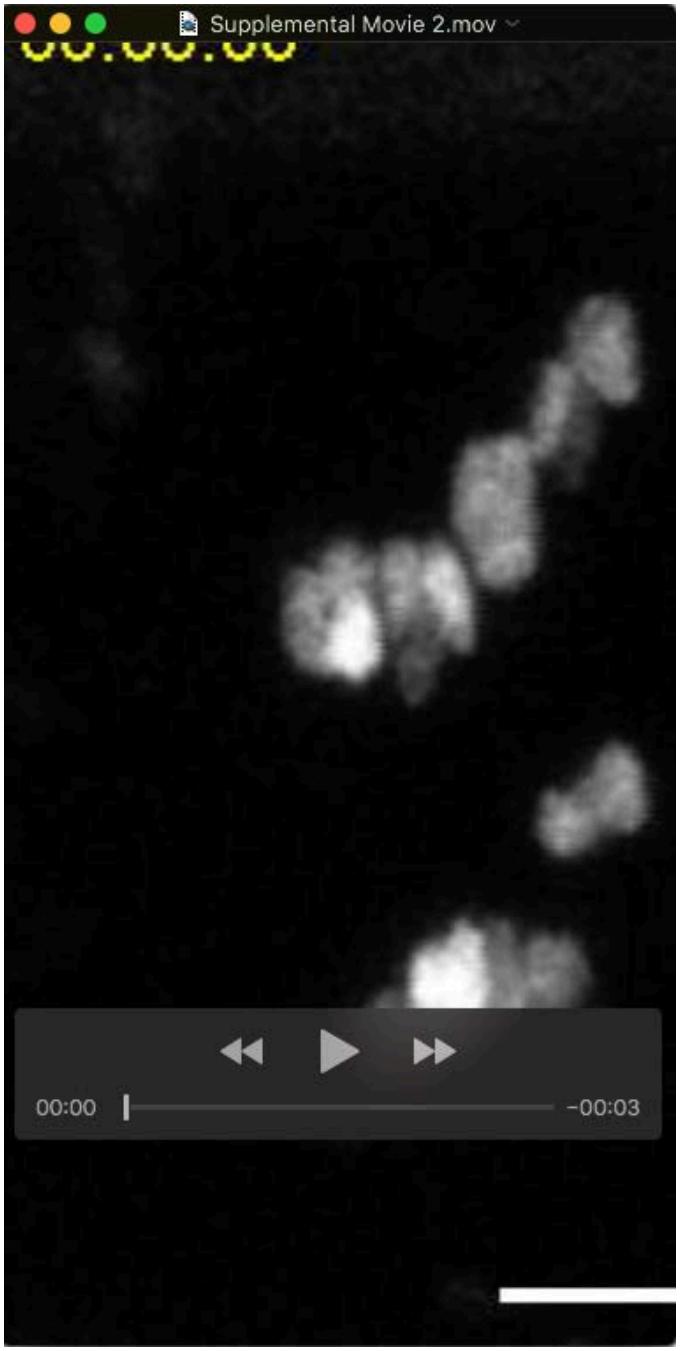

Movie S2. Myonuclear movement in control embryos

LT muscles from a *Drosophila* embryo that expressed apRed (green). Movie shows clusters of myonuclei moving toward the muscle pole in late stage 15 embryos. Time-lapse movie shown as maximum projections. Z-stacks acquired at a rate of 1 frame/2 mins. Movie plays at 10 frames/s. Scale bar, 10 µm.

Journal of Cell Science • Supplementary information

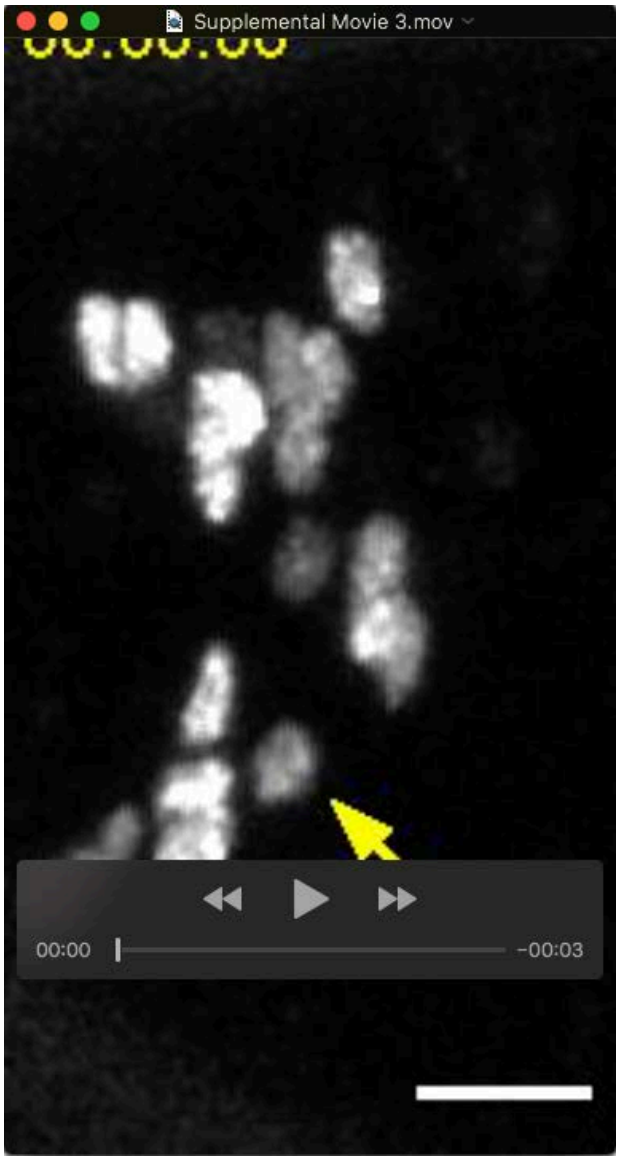

Movie S3. Myonuclei collapsing in *Aplip1*^{DG20707} embryos

LT muscles of the *Drosophila* embryo expressing apRed (green). Movie shows myonuclear collapse in ventral to dorsal direction in an LT muscle (indicated with yellow arrow). Time-lapse movie shown as maximum projections. Z-stacks acquired at a rate of 1 frame/2 mins. Movie plays at 10 frames/s. Scale bar, 10 µm.

Journal of Cell Science • Supplementary information